Received: 6 November 2017 | Revised: 28 December 2017 | Accepted: 29 December 2017

DOI: 10.1002/aoc.4289

FULL PAPER

WILEY Applied Organometallic Chemistry

Metal complexes of novel Schiff base derived from iron sandwiched organometallic and 4-nitro-1,2-phenylenediamine: Synthesis, characterization, DFT studies, antimicrobial activities and molecular docking

Walaa H. Mahmoud[1] | Reem G. Deghadi[1] | Gehad G. Mohamed[1,2]

[1]Chemistry Department, Faculty of Science, Cairo University, Giza 12613, Egypt

[2]Egypt Nanotechnology Center, Cairo University, El-Sheikh Zayed, 6th October City, 12588 Giza, Egypt

Correspondence
Walaa H. Mahmoud, Chemistry Department, Faculty of Science, Cairo University, Giza, 12613, Egypt.
Email: dr.walaa@yahoo.com

The condensation of 2-acetylferrocene with 4-nitro-1,2-phenylenediamine in a 1:1 molar ratio, resulting in formation of a novel bi-dentate organometallic Schiff base ligand (L), (2-(1-((2-amino-5-nitrophenyl)imino)ethyl)cyclopenta-2,4-dien-1-yl)(cyclopenta-2,4-dien-1-yl)iron. Also, its Cr(III), Mn(II), Fe(III), Co(II), Ni(II), Cu(II), Zn(II) and Cd(II) complexes have been synthesized. The stoichiometric ratios of the prepared compounds were estimated using elemental analysis (C, H, N, M), molar conductivity, FT-IR, UV-Vis, ^{1}H-NMR, SEM and mass spectral analysis. Furthermore, their TG and DTG properties were studied. The geometrical structure of the complexes was found to be octahedral. From spectral analysis, the Schiff base coordinated to metal ions through the azomethine and amine groups. DFT-based molecular orbital energy calculations of the synthesized ligand have been studied, in which the ligand was theoretically optimized. The Schiff base and its metal complexes have been screened for their antimicrobial activities against different bacterial and fungal species by using disc diffusion method. The anticancer activities of the ligand and its metal complexes have also been studied towards breast cancer (MCF-7) and human normal melanocytes (HFB-4) cell lines. Molecular docking was also used to identify the interaction between the Schiff base ligand and its Cd(II) complex with the active site of the receptors of breast cancer mutant oxidoreductase (PDB ID: 3HB5), crystal structure of *Staphylococcus aureus* (PDB ID: 3Q8U) and yeast-specific serine/threonine protein phosphatase (PPZ1) of *Candida albicans* (PDB ID:5JPE).

KEYWORDS
antimicrobial activities, DFT, MCF-7, molecular docking, organometallic Schiff base

1 | INTRODUCTION

Study of coordination chemistry of transition metal complexes of Schiff bases has been enhanced by the current advancements in the fields of medicine and bioinorganic chemistry.[1] Schiff base ligands with imine groups (–RC=N–) that coordinated with metal ions have many advantages and they are very popular up to now. These ligands can be easily prepared by condensation of an active amino group as nucleophile and carbonyl group as electrophile.[2,3] These Schiff bases and their metal complexes have many applications in wide ranging area such as biology including antibacterial, anticancer, antifungal, antimalarial, antioxidant and antiviral

activities.[4,5] They can be used in reduction reaction of ketones and oxidation of organic compounds. Also Schiff bases are widely used as dyes, pigments, catalysts and polymer stabilizers.[6] Organometallic compounds have been widely applied in organic synthesis in the past several decades. Large number of reports[7] on these compounds have been demonstrated their positive role in a variety of synthetic transformations or polymerizations and acting as catalysts or reagents.[8] There are only a few groups of compounds that have possessed the attention of chemists so intensively as ferrocenes. Since the discovery of this sandwich complex in 1951,[9] an excessive of its derivatives have been synthesized and characterized. In the last two decades, ferrocene has shown great undertaking in the area of medicinal organometallic chemistry.[10] Ferrocene based organometallics and metal complexes have unique properties like stability, low toxicity, aromaticity, redox activity, lipophilicity, different membrane permeation properties and anomalous metabolism. Ferrocene containing metal-chelate complexes can be regarded as multinuclear molecules possessing both the features of coordination chemistry and of organometallics. They have importance as antibacterial and antifungal activities.[11] Because the significant lipophilicity and the reversible redox properties of ferrocene, it could be better in cell permeability and stability in biological aqueous medium. It also could be suitable for designing ferrocene-based bioorganometallic species that can be used in therapeutic applications.[12] Also ferrocenyl compounds can be used as enzyme inhibitors, metabolic competitors, therapeutic agents, radiopharmaceutical and histological agents. Their potential as antitumour agents are well documented.[13] The anticancer activity of ferrocene derivatives was firstly studied in 1970, when scientists gave an account of the antitumor activity of ferrocenyl compounds containing amine or amide groups against lymphocytic leukemia. Firstly, the antitumor activity of these synthesized compounds was low but significant enough to display that the incorporation of the ferrocenyl group into an appropriate carrier could provide an agent with enhanced antitumor activity. So since then, different types of ferrocenyl compounds have been prepared and evaluated in terms of anticancer properties.[14] Schiff bases of *o*-phenylenediamine derivatives have different applications such as biological, analytical and clinical applications. These Schiff bases can be used as substrates in the synthesis of a number of biologically active and industrial compounds.[15] The present investigation was undertaken to prepare Schiff base by condensation of 2-acetylferrocene with 4-nitro-*o*-phenylenediamine. Then its coordination behavior with different transition metal ions was studied. The novel synthesized ligand and its metal complexes were characterized using different techniques. Also thermal decomposition was studied. The biological and anticancer activities of the Schiff base ligand and its complexes were investigated. Molecular docking was studied to explain the mode of binding between the organometallic Schiff base ligand (L) and the receptors of breast cancer mutant oxidoreductase (PDB ID: 3HB5), crystal structure of *Staphylococcus aureus* (PDB ID: 3Q8U)and yeast-specific serine/threonine protein phosphatase (PPZ1) of *Candida albicans* (PDB ID:5JPE).

2 | EXPERIMENTAL

2.1 | Materials and reagents

All chemicals used were of the analytical reagent grade (AR) and of highest purity available. The chemicals used included 2-acetylferrocene which was supplied from Strem Chemicals Inc., 4-nitro-*o*-phenylenediamine (Sigma-Aldrich), $CrCl_3.6H_2O$, $MnCl_2.2H_2O$ and$FeCl_3.6H_2O$ (Sigma-Aldrich, Germany), $NiCl_2.6H_2O$, $CoCl_2.6H_2O$, $CuCl_2.2H_2O$ and $ZnCl_2$ (BDH) and $CdCl_2$ (Merck, Germany). Organic solvents used were ethyl alcohol (95 %), methyl alcohol and *N,N*-dimethylformamide (DMF). Deionized water was usually used in all preparations.

2.2 | Solutions

Stock solutions of the ferrocene Schiff base ligand and its metal complexes of 1×10^{-3} M were prepared by dissolving an accurately weighed amount in *N,N*-dimethylformamide. The conductivity then measured for the metal complexes solutions. Dilute solutions of the Schiff base ligand and its metal complexes (1×10^{-4} M) were prepared by accurate dilution from the previous prepared stock solutions for measuring their UV–Vis spectra.

2.3 | Solution of anticancer study

A fresh stock solution (1×10^{-3} M) of Schiff base ligand (0.12×10^{-2} g l^{-1}) was prepared in the appropriate volume of DMF (90%). DMSO was used in cryopreservation of cells. RPMI-1640 medium was used. The medium was used for culturing and maintenance of the human tumor cell line. The medium was supplied in a powder form. It was prepared as follows: 10.4 g of medium was weighed, mixed with 2 g of sodium bicarbonate, completed to 1 l with distilled water and shaken carefully until complete dissolution. The medium was then sterilized by filtration in a Millipore bacterial filter (0.22 ml). The prepared medium was kept in a refrigerator (4 °C) and checked at regular intervals for contamination. Before use, the medium was warmed at 37 °C in a water bath and

supplemented with penicillin–streptomycin and FBS. Sodium bicarbonate was used for the preparation of RPMI-1640 medium. Isotonic trypan blue solution (0.05%) was prepared in normal saline and was used for viability counting. FBS (10%, heat inactivated at 56 °C for 30 min), 100 units/mL penicillin and 2 mg/ml streptomycin were used for the supplementation of RPMI-1640 medium prior to use. Trypsin (0.25 X 10^{-1}% w/v) was used for the harvesting of cells. Acetic acid (1% v/v) was used for dissolving unbound SRB dye. SRB (0.40%) dissolved in 1% acetic acid was used as a protein dye. A stock solution of trichloroacetic acid (50%) was prepared and stored. An amount of 50 μL of the stock was added to 200 μL of RPMI-1640 medium per well to yield a final concentration of 10% used for protein precipitation. Isopropanol (100%) and ethanol (70%) were used. Tris base (10 mM; pH = 10.50) was used for SRB dye solubilization. Tris base (121.10 g) was dissolved in 1000 ml of distilled water and the pH was adjusted using hydrochloric acid (2 M).

2.4 | Instrumentation

Microanalyses of carbon, hydrogen and nitrogen were carried out at the Microanalytical Center, Cairo University, Egypt, using a CHNS-932 (LECO) Vario elemental analyser. Analyses of the metals were conducted by dissolving the solid complexes in concentrated HNO_3, and dissolving the residue in deionized water. The metal content was carried out using inductively coupled plasma atomic absorption spectrometry (ICP-AES), Egyptian Petroleum Research Institute. Fourier transform infrared (FT-IR) spectra were recorded with a PerkinElmer 1650 spectrometer (400-4000 cm^{-1}) in KBr pellets. ^{1}H-NMR spectra, as solutions in DMSO-d_6, were recorded with a 300 MHz Varian-Oxford Mercury at room temperature using tetra-methylsilane as an internal standard. Mass spectra were recorded using the electron ionization technique at 70 eV with an MS-5988 GS-MS Hewlett-Packard instrument at the Microanalytical Center, National Center for Research, Egypt. UV–visible spectra were obtained with a Shimadzu UVmini-1240 spectrophotometer. Molar conductivities of 10^{-3} M solutions of the solid complexes in DMF were measured using a Jenway 4010 conductivity meter. Thermogravimetric (TG) and differential thermogravimetric (DTG) analyses of the solid complexes were carried out from room temperature to 1000 °C using a Shimadzu TG-50H thermal analyser. Antimicrobial measurements were carried out at the Microanalytical Center, Cairo University, Egypt. Anticancer activity experiments were performed at the National Cancer Institute, Cancer Biology Department, Pharmacology Department, Cairo University. The optical density (OD) of each well was measured spectrophotometrically at 564 nm with an ELIZA microplate reader (Meter tech. R960, USA). The scanning electron microscope (SEM) image of the complexes was recorded by using SEM Model Quanta 250 FEG (Field Emission Gun) attached with EDX unit (Energy Dispersive X-ray Analyses), with accelerating voltage 30 K.V., magnification 14X up to 1000000 and resolution for Gun.1n, National Research Center, Egypt.

2.5 | Synthesis of organometallic Schiff base ligand (L)

The organometallic Schiff base ligand (L) was prepared by refluxing a mixture of 4-nitro-*o*-phenylenediamine (0.03 mol, 4.59 g) dissolved in ethanol and 2-acetylferrocene (0.03 mol, 7 g) dissolved in methanol. The resulting mixture was stirred under reflux for about 2 h at100–150 °C, during which a dark brown solid compound was separated. It was filtered, recrystallized, washed with diethylether and dried in vacuum.

Yield 93%; m.p. 210 °C; dark brown solid. Anal. Calcd for $C_{18}H_{17}FeN_3O_2$ (%): C, 59.50; H, 4.68; N, 11.57; Fe, 15.43. Found (%): C, 59.00; H, 4.63; N, 11.95; Fe, 15.80. FT-IR (cm^{-1}): azomethine ν(C=N) 1633sh, amino group $\nu(NH_2)_{bending}$ 633w. ^{1}H NMR (300 MHz, DMSO-d_6, δ, ppm): 4.22–4.76 (m, 9H, ferrocene ring), 6.00-7.39 (m, 3H, aromatic ring), 5.02 (s, 2H, amino group), 1.20 (s, 3H, methyl group). λ_{max} (nm): 276, 328 (π –π*) and 418 charge transfer.

2.6 | Synthesis of metal complexes

The Cr(III), Mn(II), Fe(III), Co(II), Ni(II), Cu(II), Zn(II) and Cd(II) complexes were prepared by a reaction of 1:1 molar mixture of hot ethanolic solution (60 °C) of the metal chloride (1.10 X 10^{-3} mol) and the DMF solution of Schiff base ligand (L) (0.40 g, 1.10 X 10^{-3} mol). The resulting mixture was stirred under refluxing for 1 h, during which the complexes were precipitated. They were collected by filtration and purified by washing several times with diethyl ether. The solid complexes then dried in desiccator over anhydrous calcium chloride. The percent yield was ranged from 79 to 90%.

2.6.1 | $[Cr(L)(H_2O)_2Cl_2]Cl.4H_2O$

Yield 89%; m.p. >300 °C; black solid. Anal. Calcd for $C_{18}H_{29}Cl_3FeCrN_3O_8$ (%): C, 34.31; H, 4.61; N, 6.67; Fe, 8.90; Cr, 8.26. Found (%): C, 34.19; H, 4.57; N, 6.52; Fe, 8.70; Cr, 9.29. FT-IR (ν, cm^{-1}): azomethine (C=N) 1647sh, H_2O stretching of coordinated water 900w and 826 s, amino group $(NH_2)_{bending}$ 632w, (M—O coordinated water) 560 m, (M—N) 478w. UV-vis (λ_{max}, nm): 263(π–π*).

2.6.2 | $[Mn(L)(H_2O)_2Cl_2]2H_2O$

Yield 85%; m.p. >300 °C; black solid. Anal. Calcd for $C_{18}H_{25}Cl_2FeMnN_3O_6$ (%): C, 38.50; H, 4.46; N, 7.49; Fe, 9.98; Mn, 9.81. Found (%): C, 38.38; H, 4.34; N, 7.31; Fe, 9.10; Mn, 10.41. FT-IR (ν, cm^{-1}): azomethine (C=N) 1647sh, H_2O stretching of coordinated water 935 s and 848 s, amino group $(NH_2)_{bending}$ 613 s, (M—O coordinated water) 587w, (M—N) 478w. UV-vis (λ_{max}, nm): 277(π–π^*).

2.6.3 | $[Fe(L)(H_2O)_2Cl_2]Cl.2H_2O$

Yield 83%; m.p. >300 °C; grey solid. Anal. Calcd for $C_{18}H_{25}Cl_3Fe_2N_3O_6$ (%): C, 36.15; H, 4.18; N, 7.03; Fe, 18.75. Found (%): C, 36.04; H, 4.06; N, 6.70; Fe, 19.11. FT-IR (ν, cm^{-1}): azomethine (C=N) 1647sh, H_2O stretching of coordinated water 903w and 824 m, amino group $(NH_2)_{bending}$ 618 s, (M—O coordinated water) 544w, (M—N) 489w. UV-vis (λ_{max}, nm): 315 (π –π^*).

2.6.4 | $[Co(L)(H_2O)_2Cl_2]3H_2O$

Yield 90%; m.p. >300 °C; black solid. Anal. Calcd for $C_{18}H_{27}Cl_2FeCoN_3O_7$ (%): C, 37.05; H, 4.63; N, 7.20; Fe, 9.61; Co, 10.12. Found (%): C, 37.03; H, 4.54; N, 6.84; Fe, 8.52; Co, 10.68. FT-IR (ν, cm^{-1}): azomethine (C=N) 1643sh, H_2O stretching of coordinated water 913w and 821 m, amino group $(NH_2)_{bending}$ 676 s, (M—O coordinated water) 586 s, (M—N) 478w. UV-vis (λ_{max}, nm): 264(π–π^*), 307 (π –π^*), 596 and 662 (d-d splitting).

2.6.5 | $[Ni(L)(H_2O)_3Cl]Cl.2H_2O$

Yield 88%; m.p. >300 °C; black solid. Anal. Calcd for $C_{18}H_{27}Cl_2FeNiN_3O_7$ (%): C, 37.05; H, 4.63; N, 7.20; Fe, 9.61; Ni, 10.12. Found (%): C, 36.82; H, 4.48; N, 6.82; Fe, 8.37; Ni, 11.10. FT-IR (ν, cm^{-1}): azomethine (C=N) 1646sh, H_2O stretching of coordinated water 935w and 824 m, amino group $(NH_2)_{bending}$ 676w, (M—O coordinated water) 578 s, (M—N) 479w. UV-vis (λ_{max}, nm): 266 (π–π^*).

2.6.6 | $[Cu(L)(H_2O)_3Cl]Cl.H_2O$

Yield 79%; m.p. >300 °C; black solid. Anal. Calcd for $C_{18}H_{25}Cl_2FeCuN_3O_6$ (%): C, 37.93; H, 4.39; N, 7.38; Fe, 9.83; Cu, 11.15. Found (%): C, 37.54; H, 4.25; N, 7.13; Fe, 10.20; Cu, 10.67. FT-IR (ν, cm^{-1}): azomethine (C=N) 1638sh, H_2O stretching of coordinated water 935w and 824 m, amino group $(NH_2)_{bending}$ 601 s, (M—O coordinated water) 565w, (M—N) 489w. UV-vis (λ_{max}, nm): 266 (π–π^*).

2.6.7 | $[Zn(L)(H_2O)_2Cl_2]H_2O$

Yield 85%; m.p. >300 °C; black solid. Anal. Calcd for $C_{18}H_{23}Cl_2FeZnN_3O_5$ (%): C, 39.06; H, 4.16; N, 7.60; Fe, 10.13; Zn, 11.75. Found (%): C, 38.70; H, 3.88; N, 7.38; Fe, 10.74; Zn, 11.32. FT-IR (ν, cm^{-1}): azomethine (C=N) 1645sh, H_2O stretching of coordinated water 935w and 848w, amino group $(NH_2)_{bending}$ 606 s, (M—O coordinated water) 544w, (M—N) 500w. UV-vis (λ_{max}, nm): 262(π–π^*).

2.6.8 | $[Cd(L)(H_2O)_2Cl_2]$

Yield 79%; m.p. 171 °C; brown solid. Anal. Calcd for $C_{18}H_{21}Cl_2FeCdN_3O_4$ (%): C, 37.09; H, 3.61; N, 7.21; Fe, 9.61; Cd, 19.30. Found (%): C, 37.04; H, 3.45; N, 6.88; Fe, 10.20; Cd, 18.79. FT-IR (ν, cm^{-1}): azomethine (C=N) 1636sh, H_2O stretching of coordinated water 883 sand 812 s, amino group $(NH_2)_{bending}$ 612 m, (M—O coordinated water) 544w, (M—N) 486 s. ^1H NMR (300 MHz, DMSO-d_6, δ, ppm): 4.22–4.76 (m, 9H, ferrocene ring), 6.00-7.40 (m, 3H, aromatic ring), 5.08 (s, 2H, amino group). UV-vis (λ_{max}, nm): 278, 333 (π –π^*) and 422 (charge transfer).

2.7 | Spectrophotometric studies

The absorption spectra were recorded for 1 X 10^{-4} M solutions of the free organometallic Schiff base ligand and its metal complexes that dissolved in DMF. The spectra were scanned within the wavelength range from 200 to 700 nm.

2.8 | Antimicrobial activity

The tests for in vitro antibacterial and antifungal activities were performed through the disc diffusion method.[16] The bacterial organisms used were Gram (+) bacteria: [*Streptococcus mutans, Staphylococcus aureus],* Gram(−) bacteria: [*Escherichia coli, Klebsiella pneumonia, Pseudomonas aeruginosa*] and fungal specie include [*Candida albicans*]. Stock solution (0.001 mol) was prepared by dissolving the compounds in DMSO. The nutrient agar medium for antibacterial was (0.50% Peptone, 0.10% Beef extract, 0.20% Yeast extract, 0.50% NaCl and 1.50% Agar-Agar) was prepared, cooled to 47 °C and seeded with tested microorganisms. After solidification 5 mm diameter holes were punched by a sterile corkborer. The investigated compounds, i.e. Schiff base ligand and their metal complexes, were introduced in Petri-dishes (only 0.1 m) after dissolving in DMSO at 1.0 x 10^{-3} M. These culture plates were then incubated at 37 °C for 20 h for bacteria. The activity was determined by measuring the diameter of the inhibition zone (in mm). The plates were kept for incubation at 37 °C for 24 h and then the plates

were examined for the formation of zone of inhibition. The diameter of the inhibition zone was measured in millimeters. Antimicrobial activities were performed in triplicate and the average was taken as the final reading.[17]

2.9 | Anticancer activity

Potential cytotoxicity of the compounds was tested using the method of Skehan and Storeng.[18] Cells were plated in 96-multiwell plate (104 cells/well) for 24 h before treatment with the compounds to allow attachment of cell to the wall of the plate. Different concentrations of the compounds under investigation (0, 5, 12.5, 25, 50 and 100 μg/ml) were added to the cell monolayer and triplicate wells were prepared for each individual dose. The monolayer cells were incubated with the compounds for 48 h at 37 °C and in 5% CO_2 atmosphere. After 48 h, cells were fixed, washed and stained with SRB stain. Excess stain was washed with acetic acid and attached stain was recovered with tris-EDTA buffer. The optical density (O.D.) of each well was measured spectrophotometrically at 564 nm with an ELIZA microplate reader, the mean background absorbance was automatically subtracted and mean values of each drug concentration was calculated. The relation between drug concentration and surviving fraction is plotted to get the survival curve of breast tumor cell line for each compound.

Calculation:

The percentage of cell survival was calculated as follows:

Survival fraction = O.D. (treated cells) / O.D. (control cells). The IC_{50} values (the concentrations of the Schiff base ligand (L) or its metal complexes required to produce 50% inhibition of cell growth). The experiment was repeated 3 times.

2.10 | Computational methodology

DFT and molecular modeling theoretical calculations for organometallic Schiff base ligand (L) were carried out on Gaussian03 package[19] at density functional theory (DFT) level of theory. The molecular geometry for the tested ligand was fully optimized using density functional theory based on B3LYP method along with the LANL2DZ basis set. The optimized structure of the ligand (L) was visualized using Chemcraft version 1.6 package[20] and Gauss View version 5.0.9.[21] Quantum chemical parameters such as the highest occupied molecular orbital energy(E_{HOMO}), the lowest unoccupied molecular orbital energy (E_{LUMO}) and HOMO–LUMO energy gap (ΔE) for the investigated molecule were calculated.

2.11 | Molecular docking

Molecular docking studies were elaborated using MOE 2008 software. These studies are very important for predicting the possible binding modes of the most active compounds with the receptors of breast cancer mutant oxidoreductase (PDB ID: 3HB5), crystal structure of *Staphylococcus aureus* (PDB ID: 3Q8U) and yeast-specific serine/threonine protein phosphatase (PPZ1) of *Candida albicans* (PDB ID:5JPE).[22] Docking is an interactive molecular graphics program can be used to calculate and display feasible docking modes of a receptor, ligand and complex molecules. It necessitates the ligand and the receptor as PDB format input. The water molecules, co-crystallized ligands and other unsupported elements (e.g., Na, K, Hg, etc.,) were removed but the amino acid chain was kept.[23] The structure of the ligand in PDB file format was created by Gaussian03 software. The crystal structures of breast cancer mutant oxidoreductase (PDB ID: 3HB5), crystal structure of *Staphylococcus aureus* (PDB ID: 3Q8U) and yeast-specific serine/threonine protein phosphatase (PPZ1) of *Candida albicans* (PDB ID:5JPE) were downloaded from the protein data bank (http://www.rcsb.org./pdb).

3 | RESULTS AND DISCUSSION

3.1 | Characterization of organometallic Schiff base ligand (L)

A new dark brown asymmetrical Schiff base ligand (L), (2-(1-((2-amino-5-nitrophenyl)imino)ethyl)cyclopenta-2,4-dien-1-yl)(cyclopenta-2,4-dien-1-yl)iron was prepared from 2-acetylferrocene and 4-nitro-*o*-phenylenediamine. The results of elemental analysis for the Schiff base ligand were in good agreement with the calculated values that confirm its molecular formula as $C_{18}H_{17}FeN_3O_2$. The infrared (IR) spectrum has an important role for identifying the functional groups and showing significant evidence for the interaction between the starting materials to get the Schiff base ligand (L).[24] IR spectrum of ferrocene showed peaks at 1500, 3000 and 475 cm^{-1} which assigned to ν(C=C) double bond of cyclopentadienyl, ν(C-H) stretching indicating the hydrogen involved in the cyclic ring and ν(Fe-C) bond.[25] The IR spectrum of the Schiff base ligand showed the absence of a band at ~1725 cm^{-1} assigned to ν(C=O) of 2-acetylferrocene with the appearance of a new band at 1633 cm^{-1} assigned to the azomethine

group (C=N). The presence of this azomethine group suggested that the condensation process has been occurred and the Schiff base was formed.[26] Also two sharp bands were appeared at 3432 and 3400 cm^{-1} which corresponding to $\nu(NH_2)$ stretching vibration.[27] In addition, it was observed that the $\nu(NH_2)$ bending band was appeared at 633 cm^{-1}.[28] Also the Fe-C bond of the Schiff base was observed at 462 cm^{-1}.[25] ^{1}H-NMR spectrum of Schiff base ligand showed multiplet signals in the region of 4.22-4.76 ppm, which attributed to the ferrocene protons.[29] Also proton signals were observed as multiplet peak in aromatic region around 6.00-7.39 ppm. In the ^{1}H-NMR spectrum of the free ligand, the NH_2 protons signal was observed as a singlet signal at 5.02 ppm.[30] Also, the spectrum showed the protons of methyl group at 1.20 ppm.[31] The mass spectrum of the synthesized Schiff base ligand (L) was recorded and the obtained molecular ion (m/z) peak at 365 amu confirmed the proposed formula in which the ligand moiety was $C_{18}H_{17}FeN_3O_2$ with atomic mass 363 g/mol.

3.1.1 | Geometrical optimization of the Schiff base ligand

The geometrical structure of the organometallic Schiff base ligand (L) was shown in Figure 1. Also the bond lengths and bond angles were listed in (Table 1).The HOMO–LUMO energy gap (ΔE), was used to develop theoretical models for elucidating the structure and conformation barriers of the Schiff base ligand (L) in many molecular systems.[32,33] Furthermore, the calculated quantum chemical parameters of Schiff base ligand were given in Table 2. Additional parameters such as ΔE, absolute electro negativities, χ, absolute hardness, η, chemical potentials, Pi, absolute softness, σ, global softness, S, global electrophilicity, ω, and additional electronic charge, ΔN_{max} were calculated.[34]

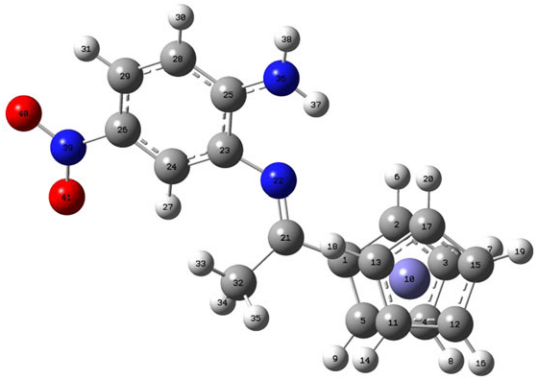

FIGURE 1 The optimized structure of organometallic Schiff base ligand (L)

From these data, it was showed that the value of ΔE for the organometallic Schiff base ligand (L) was found to be 2.80 eV. The total energy gap of free ligand was small whichindicatedthe high stability of the prepared organometallic Schiff base ligand (L).Also the positive value of electrophilicity index (χ) and the negative value of chemical potential (Pi) showed that the ligand can accept electrons from the environmentand its energy should be decrease upon accepting electronic charge.[35]

3.1.2 | Molecular electrostatic potential (MEP)

The electrostatic potential is the energy which resulted from the interaction of positive charge (an electrophile) with the electrons of a molecule. Negative electrostatic potentials indicated areas that were prone to electrophilic attack.[36] Molecular electrostatic potential (MEP) was a very useful description used for understanding sites for electrophilicor nucleophilic attack and also it was very great for studying the biological recognition process.[37] MEP surfaces were gained based on the optimized geometry, which was helpful for predicting reactive sites of nucleophilic or electrophilic attack and hydrogen bonding or weak interaction for the investigated compounds. In this investigation, MEP of the organometallic Schiff base ligand (L) was showed in Figure 2. In MEP, electrostatic potential at the surface can be represented by different colors: red colored surfaces corresponding to negative MEP that represent high electron density, while lowest electron density represented by blue colored surfaces. From MEP, the most negative regions were located around oxygen atoms of the ligand so surrounded by red colored but these atoms were present out of plane so not interring in the coordination. The regions over the benzene and ferrocene rings were neutral and represented by green color.[38]

3.1.3 | Vibrational properties

From DFT, the optimized geometry can be also used in calculating the theoretical vibrational bands of the organometallic Schiff base ligand (L). The vibrational frequencies computed at quantum chemical methods such as DFT levels that unfortunately contain systematic errors. To overcome these errors (which can be formed from harmonicity), scaling factor of 0.9648 for LanL2DZ can be used.[39,40] Figure 3 illustrated the calculated and experimental infrared spectra of the Schiff base ligand (L) inthe frequency range from 450 to 4000 cm^{-1}. The FT-IR spectra of the prepared compound showed two characteristic bands at 1633 cm^{-1} and 633 cm^{-1} which corresponding to azomethine group ν(C=N) and

TABLE 1 The different optimized parameters (bond lengths and bond angles) of organometallic Schiff base ligand (L).

Bond length (Å)			
C(12)-H(16)	1.0811	N(36)-H(37)	1.013
C(13)-C(17)	1.4423	N(36)-H(38)	1.0088
C(13)-H(18)	1.0813	N(39)-O(40)	1.2857
C(15)-C(17)	1.4437	N(39)-O(41)	1.287
C(15)-H(19)	1.0811	C(12)-H(16)	1.0811
C(17)-H(20)	1.0809	C(13)-C(17)	1.4423
C(21)-N(22)	1.3079	C(13)-H(18)	1.0813
C(21)-C(32)	1.5229	C(15)-C(17)	1.4437
N(22)-C(23)	1.4118	C(15)-H(19)	1.0811
C(23)-C(24)	1.4025	C(17)-H(20)	1.0809
C(23)-C(25)	1.4424	C(21)-N(22)	1.3079
C(24)-C(26)	1.4094	C(21)-C(32)	1.5229
C(24)-H(27)	1.0829	N(22)-C(23)	1.4118
C(25)-C(28)	1.4191	C(23)-C(24)	1.4025
C(25)-N(36)	1.3746	C(23)-C(25)	1.4424
C(26)-C(29)	1.4097	C(24)-C(26)	1.4094
C(26)-N(39)	1.4562	C(24)-H(27)	1.0829
C(28)-C(29)	1.3953	C(25)-C(28)	1.4191
C(28)-H(30)	1.0874	C(25)-N(36)	1.3746
C(29)-H(31)	1.0841	C(26)-C(29)	1.4097
C(32)-H(33)	1.0933	C(26)-N(39)	1.4562
C(32)-H(34)	1.0989	C(28)-C(29)	1.3953
C(32)-H(35)	1.0949		
Bond angle (°)			
C(2)-C(1)-C(5)	107.27	C(4)-C(5)-H(9)	125.4441
C(2)-C(1)-C(21)	125.7278	H(9)-C(5)-Fe(10)	125.8028
C(5)-C(1)-C(21)	127.0002	C(1)-Fe(10)-C(3)	66.8101
Fe(10)-C(1)-C(21)	126.004	C(1)-Fe(10)-C(4)	66.9554
C(1)-C(2)-C(3)	108.328	C(1)-Fe(10)-C(11)	125.0652
C(1)-C(2)-H(6)	124.6609	C(1)-Fe(10)-C(12)	159.8784
C(3)-C(2)-H(6)	126.9913	C(1)-Fe(10)-C(13)	110.296
H(6)-C(2)-Fe(10)	126.4596	C(1)-Fe(10)-C(15)	159.3517
C(2)-C(3)-C(4)	108.1389	C(1)-Fe(10)-C(17)	124.6762
C(2)-C(3)-H(7)	125.9692	C(2)-Fe(10)-C(4)	66.6675
C(4)-C(3)-H(7)	125.8908	C(2)-Fe(10)-C(5)	67.0197
H(7)-C(3)-Fe(10)	125.3841	C(2)-Fe(10)-C(11)	160.5109
C(3)-C(4)-C(5)	108.0677	C(2)-Fe(10)-C(12)	158.328
C(3)-C(4)-H(8)	126.0951	C(2)-Fe(10)-C(13)	125.0301
C(5)-C(4)-H(8)	125.8372	C(2)-Fe(10)-C(15)	123.4617
H(8)-C(4)-Fe(10)	125.5781	C(2)-Fe(10)-C(17)	109.371
C(1)-C(5)-C(4)	108.1932	C(3)-Fe(10)-C(5)	66.752

(Continues)

TABLE 1 (Continued)

Bond angle (°)			
C(1)-C(5)-H(9)	126.3522	C(3)-Fe(10)-C(11)	158.8501
C(3)-Fe(10)-C(12)	123.2342	C(13)-C(17)-H(20)	126.0816
C(3)-Fe(10)-C(13)	159.4189	C(15)-C(17)-H(20)	125.9373
C(3)-Fe(10)-C(15)	108.2686	C(1)-C(21)-N(22)	117.354
C(3)-Fe(10)-C(17)	123.6447	C(1)-C(21)-C(32)	117.0612
C(4)-Fe(10)-C(11)	124.1219	N(22)-C(21)-C(32)	125.583
C(4)-Fe(10)-C(12)	108.5295	C(21)-N(22)-C(23)	126.8408
C(4)-Fe(10)-C(13)	159.932	N(22)-C(23)-C(24)	125.7478
C(4)-Fe(10)-C(15)	123.084	N(22)-C(23)-C(25)	115.0754
C(4)-Fe(10)-C(17)	158.497	C(24)-C(23)-C(25)	118.829
C(5)-Fe(10)-C(11)	109.7706	C(23)-C(24)-C(26)	120.0957
C(5)-Fe(10)-C(12)	123.8374	C(23)-C(24)-H(27)	121.434
C(5)-Fe(10)-C(13)	125.2431	C(26)-C(24)-H(27)	118.4308
C(5)-Fe(10)-C(15)	158.5167	C(23)-C(25)-C(28)	119.6996
C(5)-Fe(10)-C(17)	160.4687	C(23)-C(25)-N(36)	118.1307
C(11)-Fe(10)-C(15)	66.8138	C(28)-C(25)-N(36)	122.1693
C(11)-Fe(10)-C(17)	66.7748	C(24)-C(26)-C(29)	121.5383
C(12)-Fe(10)-C(13)	66.7464	C(24)-C(26)-N(39)	118.9981
C(12)-Fe(10)-C(17)	66.8178	C(29)-C(26)-N(39)	119.463
C(13)-Fe(10)-C(15)	66.7706	C(25)-C(28)-C(29)	120.8569
Fe(10)-C(11)-H(14)	125.5727	C(25)-C(28)-H(30)	119.2355
C(12)-C(11)-C(13)	107.9715	C(29)-C(28)-H(30)	119.903
C(12)-C(11)-H(14)	125.9667	C(26)-C(29)-C(28)	118.9423
C(13)-C(11)-H(14)	126.0611	C(26)-C(29)-H(31)	119.488
Fe(10)-C(12)-H(16)	124.8851	C(28)-C(29)-H(31)	121.5659
C(11)-C(12)-C(15)	108.0132	C(21)-C(32)-H(33)	111.6586
C(11)-C(12)-H(16)	125.9964	C(21)-C(32)-H(34)	111.0283
C(15)-C(12)-H(16)	125.9875	C(21)-C(32)-H(35)	109.9736
Fe(10)-C(13)-H(18)	125.1527	H(33)-C(32)-H(34)	107.9721
C(11)-C(13)-C(17)	108.0321	H(33)-C(32)-H(35)	108.6691
C(11)-C(13)-H(18)	126.0764	H(34)-C(32)-H(35)	107.4044
C(17)-C(13)-H(18)	125.8897	C(25)-N(36)-H(37)	117.2448
Fe(10)-C(15)-H(19)	124.8799	C(25)-N(36)-H(38)	121.6105
C(12)-C(15)-C(17)	108.0021	H(37)-N(36)-H(38)	120.469
C(12)-C(15)-H(19)	125.9694	C(26)-N(39)-O(40)	118.5482
C(17)-C(15)-H(19)	126.0269	C(26)-N(39)-O(41)	118.4974
Fe(10)-C(17)-H(20)	125.4353	O(40)-N(39)-O(41)	122.954
C(13)-C(17)-C(15)	107.9809		

$\nu(NH_2)_{bending}$, respectively. The DFT calculations reproduced also two characteristic bands at 1645 cm^{-1} and 621 cm^{-1} which corresponded to ν(C=N) and $\nu(NH_2)$ bending groups, respectively. This confirmed the fact that condensation between 2-acetylferrocene and 4-nitro-1,2-phenylenediamine was occurred.

TABLE 2 The different quantum chemical parameters of organometallic Schiff base ligand (L).

The calculated quantum chemical parameters	
E (a.u)	-1134.03
Dipole moment (Debye)	8.92
E_{HOMO} (eV)	-5.75
E_{LUMO} (eV)	-2.95
ΔE (eV)	2.80
χ (eV)	4.35
η (eV)	1.40
σ $(eV)^{-1}$	0.71
Pi (eV)	-4.35
S $(eV)^{-1}$	0.36
ω (eV)	6.76
ΔN_{max}	3.11

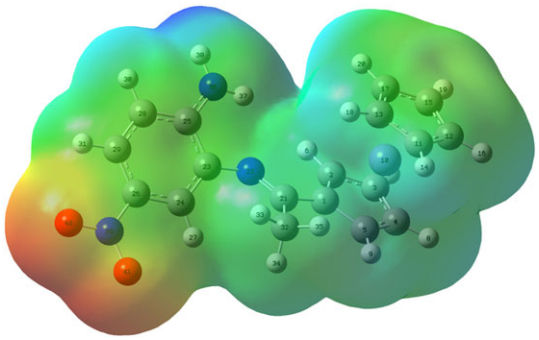

FIGURE 2 Molecular electrostatic potential map of organometallic Schiff base ligand (L). The electron density isosurface is 0.004 a.u

3.1.4 | UV-visible analysis

The electronic absorption spectral data of Schiff base ligand was recorded in 10^{-4} M DMF solution. This spectrum showed a band at 276 nm which related to the π– π * transitions of the benzene and ferrocene rings.[41] The other absorption bands at λ_{max}= 328 and 418 nm may correspond to the π–π * transition of the azomethine group and charge transfer, respectively.[42] The UV-visible spectrum of the ligand also has been calculated by using DFT. The electronic excitation energies and electronic absorption wavelengths (λ) have been computed using the DFT with optimized structure. The theoretical UV-Vis spectrum showed three important absorption bands: 279, 360 and 443 nm. The theoretical and experimental bands were shown in Figure 4. The band appeared at 279 nm with an oscillator strength of f = 0.21 correspond to the transition of HOMO-5to LUMO+1. The peak computed at 360 nm with an oscillator strength of f = 0.19 was arised from the contribution of HOMO-3 → LUMO. Finally, the peak at 443 nm correspond to transition from HOMO-2 to LUMO, was appeared with an oscillator strength of f = 0.12.[43] These results were listed in Table 3 and shown in Figure 5.

3.2 | Characterization of metal complexes

A novel bidentate organometallic Schiff base ligand (L) was synthesized by condensation of 2-acetylferrocene with 4-nitro-*o*-phenylenediamine. Among transition metal ions, Cr(III), Mn(II), Fe(III), Co(II), Ni(II), Cu(II), Zn(II) and Cd(II) complexes with the synthesized ligand were prepared. These prepared compounds were characterized by using elemental analysis (C, H, N and metal content), IR, ^{1}H-NMR, molar conductance, UV-Vis, mass, SEM and thermal analyses (TG and DTG). The structures of the metal complexes were found in Figure 6.

3.2.1 | Elemental analysis

From the data, all compounds elucidated a good agreement with the calculated values and suggested a 1:1 metal-to-ligand stoichiometric ratio for all prepared complexes. The ligand and its metal complexes had high melting points and they were stable in air. Also they were soluble in DMF and DMSO but insoluble in methanol, ethanol and water.

3.2.2 | Molar conductivity measurements

The conductivity measurements play a serious role in detection the place of counter ions either outside or inside the coordination sphere. This method was used to determine the degree of ionization of the complexes comparing to the free ligands, with the higher molar conductance value corresponding to the presence of counter ions outside the coordination sphere and vice versa. The Cr(III), Fe(III), Ni(II) and Cu(II) complexes showed molar conductivity values of75, 54, 53 and 50 Ω^{-1} mol^{-1} cm^2 in DMF solution, respectively. These results proved the monomeric and electrolytic natures of the complexes.[44] The Mn(II), Co(II), Zn(II) and Cd(II) complexes showed conductivity values below 50 Ω^{-1} mol^{-1} cm^2 such that33, 18, 14 and 2 Ω^{-1} mol^{-1} cm^2, respectively, which indicated the non-electrolytic characters of the complexes.[45]

3.2.3 | IR spectra

For detecting the coordination sites that may be involved in chelation and get preliminary conformation of the

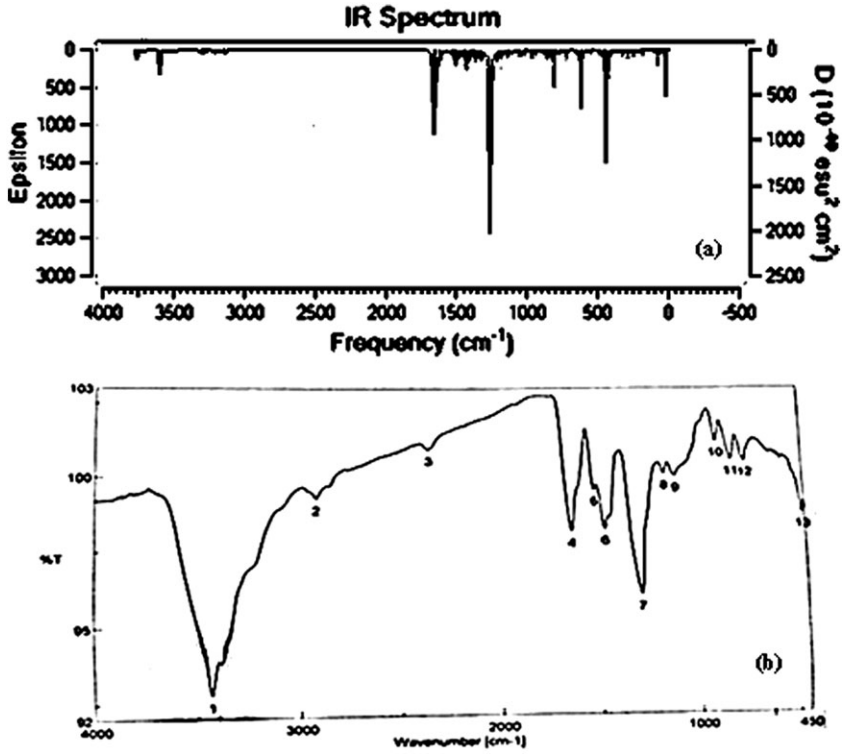

FIGURE 3 IR spectra of organometallic Schiff base ligand (L) (a) theoretical spectrum and (b) experimental spectrum

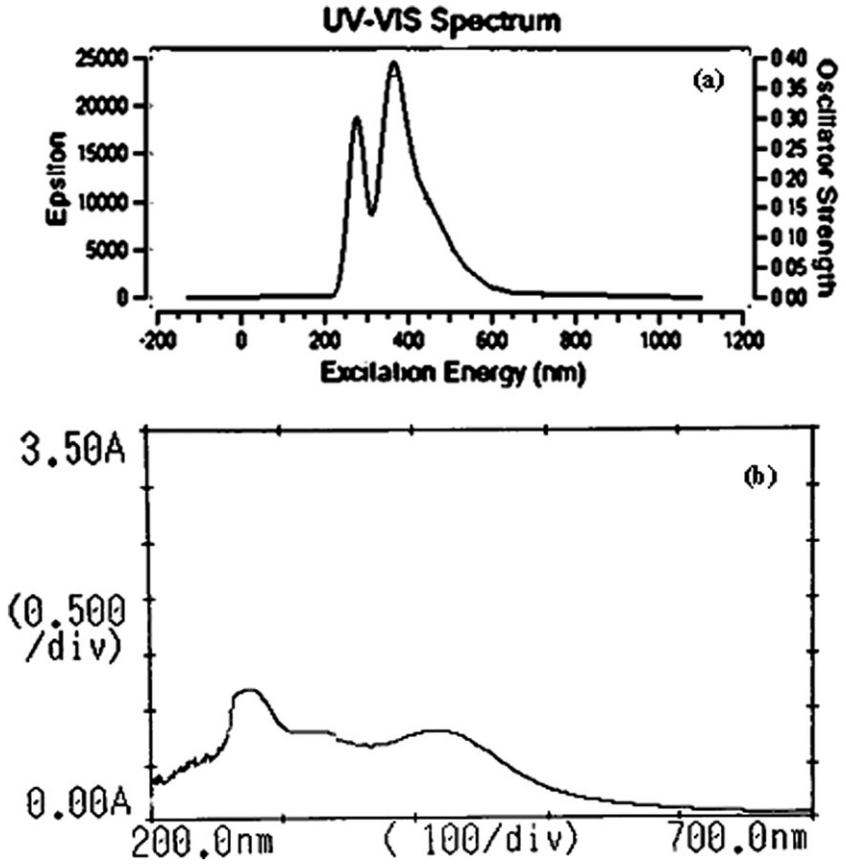

FIGURE 4 UV-visible spectra of Schiff base ligand (L) (a) theoretical spectrum and(b) experimental spectrum

structural aspects of new metal complexes, the IR spectra of the complexes were compared with that of the free Schiff base ligand. The IR spectrum of the Schiff base ligand showed disappearance of the ν(C=O) of 2-acetylferrocene and illustrated a new intense band at 1633 cm^{-1}, which can be assigned to the stretching

TABLE 3 Main calculated optical transitions with composite ion in terms of molecular orbitals.

Compound	Transition	Excitation energy (eV)	λ_{max} calcd nm/(eV)	λ_{max} exp nm/(eV)	Oscillator strength
Ligand (L)	HOMO-5 → LUMO+1 (49%)	5.24	279 (4.45)	276 (4.50)	0.21
	HOMO-3 → LUMO (61%)	3.86	360 (3.45)	328 (3.78)	0.19
	HOMO-2 → LUMO(66%)	3.05	443 (2.80)	418 (2.97)	0.12

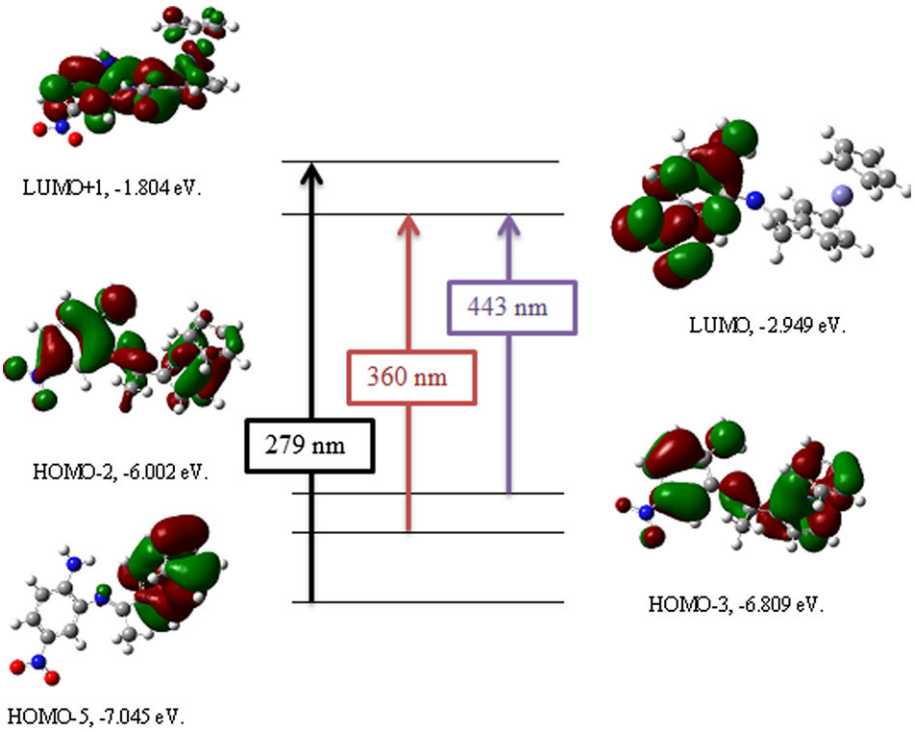

FIGURE 5 Theoretical electronic absorption transitions for Schiff base ligand (L) in DMF solvent

vibration of the ν(C=N) group. This confirmed the formation of the Schiff base ligand (L).[46] This band shifted to higher frequencies in the metal complexes in the range of 1636–1647 cm^{-1}, indicating strongly involvement of azomethine group in the coordination process.[26] Also the spectrum of ligand showed bands at 3432 and 3400 cm^{-1} which corresponding to $\nu(NH_2)$ group. Due to the presence of water molecules in the structure of all metal complexes, so these bands of amino group were included in a broad envelope band of OH group of these water molecules.[47] Furthermore, it must be detect the $\nu(NH_2)_{bending}$ band of all compounds. It was observed that the $\nu(NH_2)_{bending}$ band was appeared at 633 cm^{-1} in the free Schiff base ligand while in its metal complexes, it was shifted to appear in the range of 601-676 cm^{-1}.[28] New bands appeared at 883–935 and 812–848 cm^{-1} which can be assigned to asymmetric and symmetric vibrations of coordinated water molecules, respectively. The metal complexes demonstrated new bands in the region of 478–500 cm^{-1} and 544–587 cm^{-1}, which can be attributed to the formation of M–N and M–O (coordinated water), respectively.[48] The synthesized organometallic Schiff base ligand behaves as a neutral bidentate ligand where it binds to the central metal ions through N-azomethine and N-amino groups.

3.2.4 | ^{1}H-NMR spectra

The novel organometallic Schiff base ligand (L) and its Cd(II) complex were also supported by the ^{1}H-NMR spectral study. These spectra were recorded in DMSO-d_6. The ^{1}H-NMR spectrum of the ligand showed multiple signals within the range 6.00–7.39 ppm which assigned to the aromatic protons. These signals still appeared in the Cd(II) complex within range 6.00-7.40 ppm.[49] Other multiple signals with the integration corresponding to 9H at 4.22-4.76 ppm appeared at Schiff base ligand spectrum. These bands were assigned to the ferrocene protons. These peaks appeared at the same position in the Cd(II) complex.[50] The NH_2 proton signal appeared in the ligand at 5.02 ppm. This band shifted to higher value at 5.08 ppm in the Cd(II) complex, indicating the involvement of NH_2 group in coordination.[51]

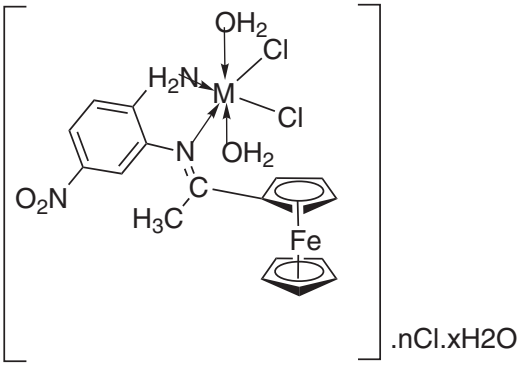

M = Cr(III); n = 1, x = 4
Mn(II); n = 0, x = 2
Fe(III); n = 1, x = 2
Co(II); n = 0, x = 3
Zn(II); n = 0, x = 1
Cd(II); n = 0, x = 0

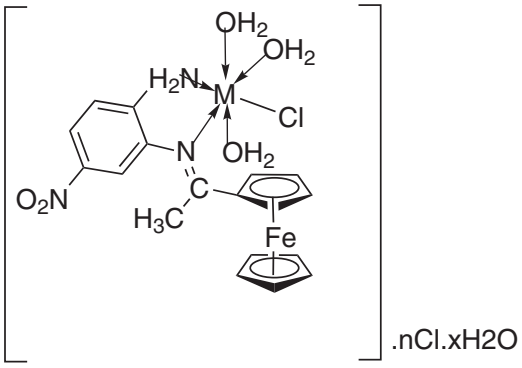

M = Ni(II); n = 1, x = 2
Cu(II); n = 1, x = 1

FIGURE 6 The structure of organometallic Schiff base metal complexes

3.2.5 | Powder X-ray diffraction studies (Powder-XRD)

The prepared complexes weren't single crystals, so it was difficult to get the XRD structure. As a result the powder diffraction data were obtained for structural characterization. In order to get the degree of crystallinity of the prepared compounds, the powder X-ray diffraction pattern of the ligand, Cr(III), Mn(II), Fe(III), Cu(II), Ni(II), Co(II), Zn(II) and Cd(II) complexes were performed. The powder X-ray diffraction pattern of all compounds was scanned in the range 3-80° (Θ) at wavelength 1.54 Å. Also, the diffractogram and the associated data describe the interplanar spacing (d-values), 2θ value for each peak and relative intensity.[52]

Crystalline peaks are not seen in the powder XRD pattern of ligand (L), Cr(III), Fe(III), Ni(II), Cd(II) and Zn(II) complexes. This indicated amorphous nature of the complexes. While Co(II), Mn(II) and Cu(II) complexes had these crystalline peaks, indicating the crystalline nature of these complexes

The average crystallite size (ξ) can be calculated from the XRD pattern according to Debye-Scherrer equation[53]:

$$\xi = \frac{K\lambda}{\beta_{1/2}\cos\theta}. \quad (1)$$

The equation contains the reference peak width at angle (θ), where λ is wavelength of X-ray radiation (1.542475 Å), K is constant taken as 0.95 for organic compounds and $\beta_{1/2}$ is the width at half maximum of the reference diffraction peak expressed in radians. The dislocation density,δ, is the number of dislocation lines per unit area of the crystal. The value of δ is related to the average particle diameter (ξ) by the relation[54,55]:

$$\delta = \frac{1}{D^2} \quad (2)$$

The value of ξ was calculated and found to be 23.58, 20.33 and 17.78 nm while the value of ξ was $1.80\text{x}10^{-3}$, $2.42\text{x}10^{-3}$ and $3.16\text{x}10^{-3}$ nm^{-2} for Co(II), Mn(II) and Cu(II) complexes, respectively.

3.2.6 | Scanning electron microscope (SEM)

The morphology, size and structure of the nanomaterials were conducted using field emission scanning electron microscopy (SEM).[40] The SEM micrographs of the Schiff base ligand (L) and its $[Cd(L)(H_2O)_2Cl_2]$ complex were presented in Figure 7. SEM images showed that the particles were agglomerated with controlled morphological structure.[56] It was evident from the SEM study that in the synthesized Cd(II) complex, crystals were found to grow up from just a single molecule to several molecules in an aggregate distribution with particle sizes that present in nanometers structures. As well, different characteristic shape of Cd(II) complex was identified and this SEM image was quite different from that of the Schiff base. The difference in the shape of the Schiff base metal complex was mainly dependent on the presence of metal ion.[57]

The micrograph of the ligand indicated collected clouds shaped particles. The Cd(II) complex showed non-uniform clusters structure. The average particle size of the ligand was 73 nm, but the average particle size of the $[Cd(L)(H_2O)_2Cl_2]$ complex was 61 nm. The synthesized nanopartical sized complex may help strongly in different fields including biological applications.[58]

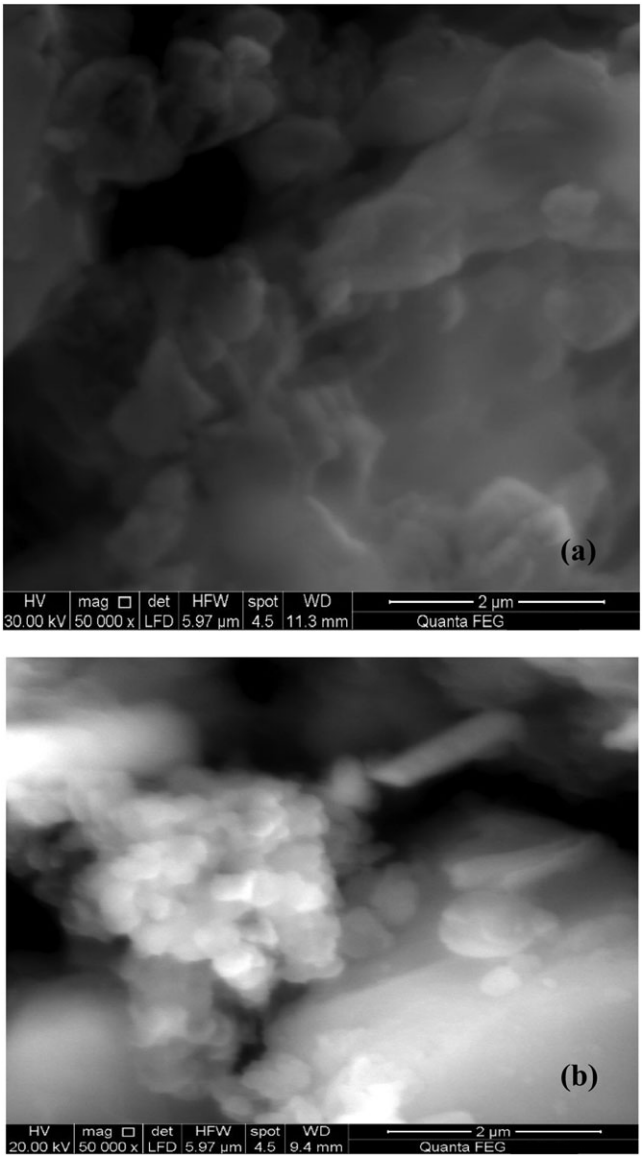

FIGURE 7 The SEM images of the nanoparticles produced a) organometallic Schiff base ligand (L) and b) $[Cd(L)(H_2O)_2Cl_2]$ complex

3.2.7 | UV-visible spectra of the Schiff base ligand and its metal complexes

The UV–Vis spectra of the ligand and its metal complexes were measured at room temperature in the region of 200–700 nm. The absorption spectrum of the Schiff base ligand (L) showed three absorption bands at 276, 328 and 418 nm. The first high intensity band was appeared at λ_{max} = 276 nm may be attributed to the π-π* transition of the aromatic rings. The second and third absorption bands that were showed at λ_{max}= 328 and 418 nm attributed to the π-π* transition of the azomethine group (C=N) and charge transfer, respectively.[44,47] Electronic spectra of the complexes showed bands which were shifted from the free ligand to 262-278 nm and 307-333 nm for π-π* of aromatic rings and π-π* of azomethine transitions, respectively, confirming the coordination of the azomethine nitrogen to the metal ions. These can be related to the binding of these coordination centers to the central metal ions. Also a band appeared at 422 nm in the Cd(II) complex corresponding to charge transfer. Furthermore, two absorption bands in the visible region of Co(II) complex were observed at 596 and 662 nm. These bands were considered to arise from the forbidden d–d splitting, which was generally too weak.[10]

3.2.8 | Mass spectra

The stoichiometry of the novel organometallic Schiff base ligand and its $[Cd(L)(H_2O)_2Cl_2]$ complex were ascertained from electron impact (EI)-mass spectral analysis. The ES-mass spectra of the compounds were elucidated their molar weight. It was found that mass spectra at 70 eV of the compounds were in good agreement with the proposed structures. The spectra of the ligand and Cd(II) complex exhibited a molecular ion peak at m/z 365 amu and 583 amu corresponding to their molecular weights 363 and 582 g/mol, respectively. The other peaks appeared in the mass spectra of the ligand and its Cd(II) complex (abundance range 1–100%) were attributed to the fragmentation of the compounds obtained from the rupture of different bonds inside the molecule.

3.2.9 | Thermal analysis of Schiff base ligand and its metal complexes

In the present investigation, the thermal stability of the Schiff base ligand (L) and its metal complexes were investigated using thermogravimetric technique (TG) and differential thermogravimetric (DTG) analyses at a heating rate of 10 °C/min in nitrogen atmosphere over the range from ambient temperature to 1000 °C. The data in (Table 4) provided information concerning thermal decomposition of these complexes in solid state. The organometallic Schiff base ligand (L) with the molecular formula ($C_{18}H_{17}FeN_3O_2$) was thermally decomposed in two successive decomposition steps. The first step with estimated mass loss of 32.28% (calculated mass loss = 32.23%) within the temperature range 75–485 °C may be attributed to the loss of $C_7H_5N_2$ molecule. The DTG curve gave maximum peak temperature at 219 °C. The second step occurred within the temperature range 485–1000 °C with an estimated mass loss 18.58% (calculated mass loss = 18.18%), which correspond to the loss of $C_2H_{12}NO$ fragment. The DTG curve gave peak at 752 °C. Finally FeO contaminated with carbon remain as residues. The overall weight loss amounted to 50.86% (calculated mass loss = 50.41%).

TABLE 4 Thermoanalytical results (TG and DTG) of organometallic Schiff base ligand (L) and its metal complexes.

Complex	TG range (°C)	DTG_{max} (°C)	n*	Mass loss Total mass loss Estim (Calcd) %	Assignment	Residues
Schiff base ligand (L)	75-485	219	1	32.28 (32.23)	-Loss of $C_7H_5N_2$.	FeO+9C
	485-1000	752	1	18.58 (18.18)	-Loss of $C_2H_{12}NO$.	
				50.86 (50.41)		
$[Cr(L)(H_2O)_2Cl_2]Cl.4H_2O$	50-340	89, 266	2	22.23 (22.72)	-Loss of $Cl_2$and $4H_2O$.	FeO $+^1/_2Cr_2O_3$
	340-1000	899	1	54.44 (53.77)	-Loss of HCl and $C_{18}H_{20}N_3O_{1.5}$.	
				76.67 (76.49)		
$[Mn(L)(H_2O)_2Cl_2]2H_2O$	30-100	79	1	7.27(6.42)	-Loss of $2H_2O$.	FeO+MnO+7C
	100-570	186, 260	2	28.37 (28.70)	-Loss of $2H_2O$,Cl_2 and C_3H_4N.	
	570-1000	760	1	24.08 (24.42)	-Loss of $C_8H_{13}N_2$.	
				59.72 (59.54)		
$[Fe(L)(H_2O)_2Cl_2]Cl.2H_2O$	30-155	63, 150	2	5.79 (6.02)	.-Loss of $2H_2O$.	FeO+$^1/_2Fe_2O_3$ +10C
	155-290	254	1	12.85 (12.38)	-Loss of H_2O,C_4H_8.	
	290-1000	707, 816	2	36.13 (36.07)	-Loss of Cl_2,$C_4H_{11}N_3O_{0.5}Cl$.	
				54.77 (54.47)		
$[Co(L)(H_2O)_2Cl_2]3H_2O$	30-290	68, 266	2	19.24 (19.90)	-Loss of $5H_2O$ and CN.	FeO+CoO+9C
	290-1000	730	1	36.70 (36.36)	-Loss of Cl_2 and $C_8H_{17}N_2$.	
				55.94 (56.26)		
$[Ni(L)(H_2O)_3Cl]Cl.2H_2O$	30-120	80	1	5.32(6.18)	-Loss of $2H_2O$.	FeO+NiO+2C
	120-640	268, 339	2	28.84 (28.30)	-Loss of Cl_2,$3H_2O$ and C_3H_4.	
	640-1000	847	1	36.34 (36.19)	-Loss of $C_{13}H_{13}N_3$.	
				70.50 (70.67)		
$[Cu(L)(H_2O)_3Cl]Cl.H_2O$	50-315	94, 264	2	19.39 (18.90)	-Loss of $4H_2O$ and ½ Cl_2.	FeO+CuO+9C
	315-640	577	1	15.42 (15.72)	-Loss of C_3H_4NCl.	
	640-1000	845	1	19.87 (19.84)	-Loss of $C_6H_{13}N_2$.	
				54.68 (54.46)		
$[Zn(L)(H_2O)_2Cl_2]H_2O$	30-200	74	1	3.43 (3.26)	-Loss of H_2O.	FeO+ZnO+10C
	200-490	241	1	13.89 (14.10)	-Loss of $2H_2O$ and C_3H_6.	
	490-745	666	1	18.29 (18.26)	-Loss of C_2H_6 and Cl_2.	
	745-1000	846	1	15.02 (15.01)	-Loss of $C_3H_5N_3$.	
				50.63 (50.63)		
$[Cd(L)(H_2O)_2Cl_2]$	75-245	222	1	16.06 (16.74)	-Loss of $2H_2O$, C_2H_2Cl.	CdO+FeO
	245-630	608	1	26.88 (26.35)	-Loss of $C_7H_6N_2Cl$.	
	630-1000	691, 877	2	22.70 (22.49)	-Loss of C_9H_9N.	
				65.64 (65.58)		

n* = number of decomposition steps

The Cr(III) complex thermally decomposed in two stages. The first stage correspond to two steps with estimated mass loss of 22.23% (calculated mass loss = 22.72%) within the range 50–340 °C and represented the loss of Cl_2 gas and four molecules of water of hydration. The second stage correspond to estimated mass loss of 54.44% (calculated mass loss =53.77%) within the range 340–1000 °C and represented the loss of HCl and $C_{18}H_{20}N_3O_{1.5}$molecules, leaving FeO and ½ Cr_2O_3 as residues. The overall weight loss amounted to 76.67% (calculated mass loss = 76.49%).

In the TG curve of Mn(II) complex, the first step displayed a gradual mass loss of 7.27% (calculated mass loss = 6.42%) within the temperature range of 30–100 °C which may be attributed to the loss of two molecules of water of hydration. The DTG curve gave peak at 79 °C (the maximum peak temperature). The second and third steps showed a mass loss of 28.37% (calculated mass loss =28.70%) which correspond to loss of $2H_2O$, Cl_2 and C_3H_4N molecules within temperature range 100–570 °C. Two maximum peaks temperatures were found at 186 °C and 260 °C. The final step was correspond to loss of $C_8H_{13}N_2$ molecule with estimated mass loss = 24.08% (calculated mass loss = 24.42%) within temperature range from 570 °C to 1000 °C. The maximum peak temperature was found at 760 °C. Finally FeO and MnO contaminated

with carbon remained as residues. The overall weight loss amounted to 59.72% (calculated mass loss = 59.54%).

The thermogram of the Fe(III) complex showed five decomposition steps within the range 30–1000 °C. The first and second decomposition steps were accompanied by loss of $2H_2O$ molecules in the range 30–155 °C with an estimated mass loss of 5.79% (calculated mass loss = 6.02%). The DTG curve gave two peaks at 63 and 150 °C (the maximum peaks temperature). The third step of decomposition correspond to loss of H_2O and C_4H_8 molecules at 155–290 °C with an estimated mass loss of 12.85% (calculated mass loss = 12.38%) with maximum peak temperature at 254 °C. The final two decomposition steps within the range 290–1000 °C were assigned to loss of Cl_2 and $C_4H_{11}N_3O_{0.5}Cl$ molecules with a mass loss of 36.13% (calculated mass loss = 36.07%). These peaks appeared at 707 and 816 °C. Thereafter the percentage of the residues correspond to ferric and ferrous oxides contaminated with carbon were 45.22% (calculated mass loss = 45.52%). The overall weight loss amounted to 54.77% (calculated mass loss = 54.47%).

The $[Co(L)(H_2O)_2Cl_2]3H_2O$ complex lost upon heating $5H_2O$ and CN in the first and second steps of decomposition within the temperature range of 30–290 °C, at maximum peaks temperatures 68 and 266 °C with estimated mass loss of 19.24% (calculated mass loss = 19.90%). The third step accounted for the loss of Cl_2 gas and $C_8H_{17}N_2$ molecule within the temperature range of 290–1000 °C, at maximum peak temperature 730 °C, with estimated mass loss of 36.70% (calculated mass loss = 36.36%), leaving FeO + CoO contaminated with carbon as residue of decomposition. The overall weight loss amounted to 55.94% (calculated mass loss = 55.26%).

The Ni(II) complex gave decomposition pattern started at 30 °C and finished at 1000 °C with three stages. The first stage was one step within the temperature range of 30–120 °C with maximum peak temperature at 80 °C and represented the loss of $2H_2O$ (hydrated) with a found mass loss of 5.32% (calculated mass loss = 6.18%). The second stage was two steps and represented the loss of Cl_2, $3H_2O$ and C_3H_4 molecules with a mass loss of 28.84% (calculated mass loss = 28.30%) within the temperature range 120–640 °C and maxima peaks temperature at 268 and 339 °C. The final stage was one step representing the loss of $C_{13}H_{13}N_3$ molecule with a mass loss of 36.34% (calculated mass loss = 36.19%) within the temperature range 640–1000 °C. At the end of the thermogram, the metal oxide NiO and FeO contaminated with carbon were the residues, which was in good agreement with the calculated metal content obtained and the results of elemental analyses. The overall weight loss amounted to 70.50% (calculated mass loss = 70.67%).

The TG curve of the Cu(II) complex showed that the first and the second decomposition steps correspond to mass loss 19.39% (calculated mass loss = 18.90%) which occurred within the temperature range from 50 to 315 °C with maximum peaks temperatures at 94 and 264 °C and represented the loss of $½Cl_2$ and $4H_2O$ molecules. The third step within the temperature range 315–640 °C with maximum peak temperature at 577 °C may be attributed to the decomposition of C_3H_4NCl molecule with found mass loss of 15.42% (calculated mass loss = 15.72%). The final step started at 640 °C and ended at 1000 °C with maximum peak temperature at 845 °C and may be accounted to the loss of $C_6H_{13}N_2$ molecule with mass loss of 19.87% (calculated mass loss = 19.84%), leaving behind CuO and FeO oxides contaminated with carbon as residues of decomposition. The overall weight loss amounted to 54.68% (calculated mass loss = 54.46%).

For Zn(II) complex, the first step of decomposition correspond to mass loss of 3.43% (calculated mass loss = 3.26%) within the temperature range 30-200 °C with maximum peak temperature at 74 °C and represented the loss of one hydrated water molecule. The second step within the temperature range 200–490 °C with maximum peak temperature at 241 °C may be attributed to the decomposition of $2H_2O$ and C_3H_6 molecules with found mass loss of 13.89% (calculated mass loss = 14.10%). The third step started at 490 °C and ended at 745 °C with maximum peak

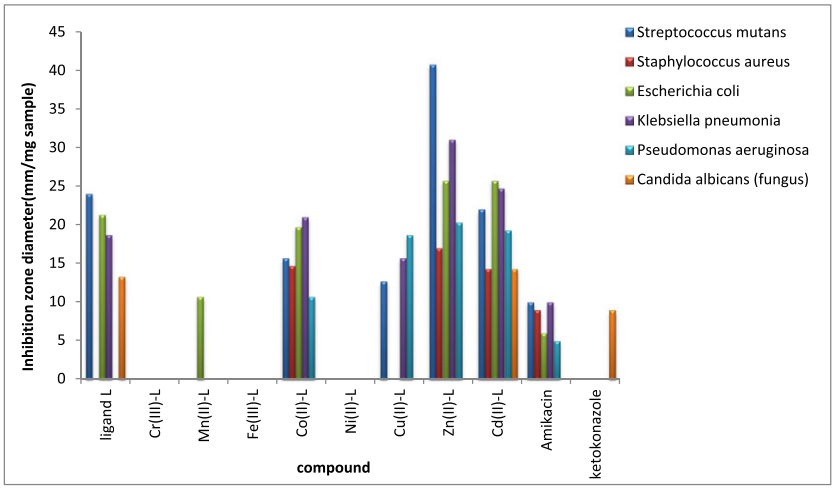

FIGURE 8 Biological activity of organometallic Schiff base ligand (L) and its metal complexes

temperature at 666 °C and may be accounted to the loss of Cl_2gas and C_2H_6 molecule with mass losses of 18.29% (calculated mass loss = 18.26%). The final step started at 745 °C and ended at 1000 °C with maximum peak temperature at 846 °C and may be accounted to the loss of $C_3H_5N_3$ molecule with mass losses of 15.02% (calculated mass loss = 15.01%), leaving behind ZnO and FeO oxides contaminated with carbon as residues of decomposition. The overall weight loss amounted to 50.63% (calculated mass loss = 50.63%).

The $[Cd(L)(H_2O)_2Cl_2]$ complex upon heating lost C_2H_2Cl and $2H_2O$ molecules in the first step of decomposition within the temperature range 75–245 °C, with a mass loss = 16.06% (calculated mass loss = 16.74%). The second step of decomposition occurred with maximum peak temperature at 608 °C and correspond to loss of $C_7H_6N_2Cl$ molecule with a mass loss = 26.88% (calculated mass loss = 26.35%), in the temperature range of 245-630 °C. The final two steps started decomposition at 630 °C and ended at 1000 °C with maximum peaks temperatures at 691 and 877 °C and may be correspond to the loss of C_9H_9N molecule with mass loss of 22.70% (calculated mass loss = 22.49%), leaving CdO and FeO oxides as residues of decomposition. The overall weight loss amounted to 65.64% (calculated mass loss = 65.58%).

As a result of these decompositions, the oxide residues always contaminated with carbon. This may be evidence of the high stability of the synthesized compounds against high temperature.

4 | STRUCTURAL INTERPRETATION

The structures of organometallic Schiff base ligand (L) and its metal complexes were characterized using various physico-chemical and spectral data. Accordingly, the structures of the complexes have been confirmed and the proposed structural formulas of the complexes were shown in (Figure 6).

4.1 | Antimicrobial activities

All the newly synthesized organometallic Schiff base ligand (L) and its metal complexes were screened for their antifungaland antibacterial activities. The tested compounds showed variable antibacterial activity against both Gram(+) bacteria: [*Streptococcus mutans, Staphylococcus aureus],* Gram (−) bacteria: [*Escherichia coli, Klebsiella pneumonia and Pseudomonas aeruginosa*] and fungal species such as *Candida albicans*. The efficiencies of the Schiff base ligand (L) and its complexes have been tested against two Gram (+ve), three Gram (−ve) and one fungi (Figure 8). Also these activities were listed in Table 5. The

TABLE 5 Biological activity of organometallic Schiff base ligand (L) and its metal complexes.

	Inhibition zone diameter (mm / mg sample)					
	(Gram positive)		*(Gram negative)*			
Sample	***Streptococcus mutans***	***Staphylococcus aureus***	***Escherichia coli***	***Klebsiella pneumonia***	***Pseudomonas aeruginosa***	***Candida albicans (fungus)***
Control: DMSO	0	0	0	0	0	0
Schiff base ligand (L)	24.0±1.0	NA	21.3±0.6	18.7±0.6	NA	13.3±1.5
$[Cr(L)(H_2O)_2Cl_2]Cl.4H_2O$	NA	NA	NA	NA	NA	NA
$[Mn(L)(H_2O)_2Cl_2]2H_2O$	NA	NA	10.7±0.6	NA	NA	NA
$[Fe(L)(H_2O)_2Cl_2]Cl.2H_2O$	NA	NA	NA	NA	NA	NA
$[Co(L)(H_2O)_2Cl_2]3H_2O$	15.7±0.6	14.7±0.5	19.7±0.6	21.0±1.0	10.7±0.5	NA
$[Ni(L)(H_2O)_3Cl]Cl.2H_2O$	NA	NA	NA	NA	NA	NA
$[Cu(L)(H_2O)_3Cl]Cl.H_2O$	12.7±0.5	NA	NA	15.7±0.5	18.7±0.6	NA
$[Zn(L)(H_2O)_2Cl_2]H_2O$	40.7±0.6	17.0±1.0	25.7±0.6	31±1.0	20.3±0.6	NA
$[Cd(L)(H_2O)_2Cl_2]$	22.0±1.0	14.3±0.5	25.7±0.6	24.7±0.6	19.3±0.6	14.3±0.6
Amikacin	10	9	6	10	5	-----
Ketokonazole	------	------	------	------	------	9

NA: No activity

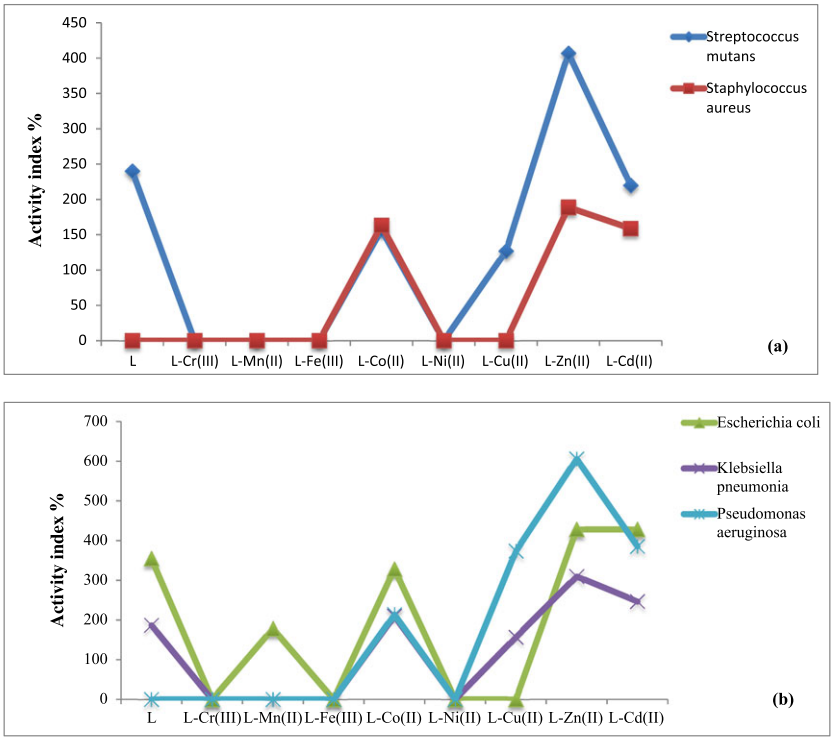

FIGURE 9 Activity index of organometallic Schiff base ligand (L) and its metal complexes against (a) different Gram positive bacteria species (b) different Gram negative bacteria species

TABLE 6 Anticancer activity of organometallic Schiff base ligand (L) and its metal complexes against breast cancer cell line.

Complex	Concn.(μg/ mL)	Surviving fraction (MCF7) 0.0	5.0	12.5	25.0	50.0	$IC_{50>}$ (μg/mL)
Schiff base ligand (L)		1.0	0.893	0.843	0.693	0.529	50.200
$[Fe(L)(H_2O)_2Cl_2]Cl.2H_2O$		1.0	0.929	0.914	0.850	0.700	
$[Co(L)(H_2O)_2Cl_2]3H_2O$		1.0	0.807	0.744	0.643	0.500	50.000
$[Cu(L)(H_2O)_3Cl]Cl.H_2O$		1.0	0.964	0.801	0.793	0.564	
$[Cd(L)(H_2O)_2Cl_2]$		1.0	0.840	0.671	0.593	0.529	50.000

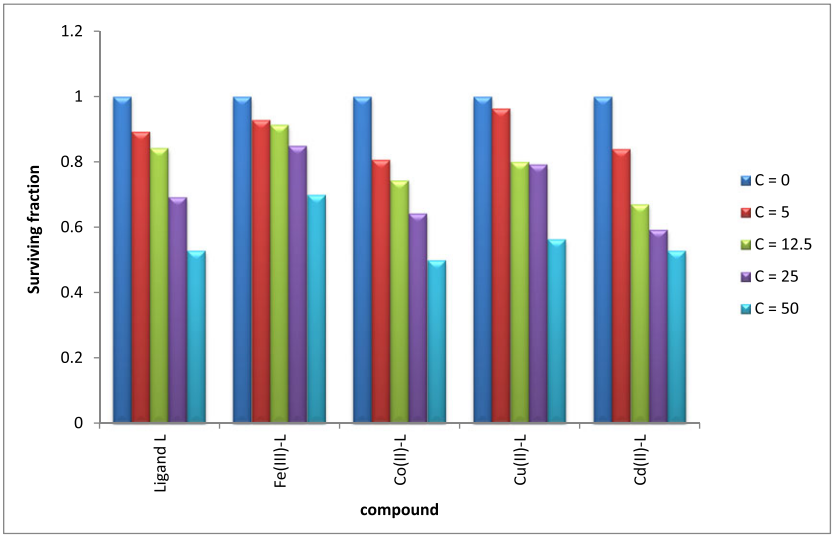

FIGURE 10 Anticancer activity of the ligand (L) and its metal complexes against breast cancer cell line

activities of the prepared Schiff base ligand and its metal complexes were confirmed by calculating the activity index according to the following relation.[59,60]

$$\text{Activity index (A)} = [\text{Inhibition Zone of compound (mm)}/\text{Inhibition Zone of standard drug (mm)}]\times 100$$

From the data, it was concluded that Zn(II) complex had the highest activity index, while Cr(III), Fe(III) and Ni(II) complexes had no activity index, Figure 9.[61]

The results from the biological activities showed that the Zn(II), Cd(II) and Co(II) complexes had higher activities against all different bacterial species than the other complexes. Zn(II) complex had the highest activity value against *streptococcus mutans* specie. Also this value was higher than the Schiff base ligand and ampicillin standard. So, Zn(II) complex can be used as very active drug against *streptococcus mutans* specie. But, each of Cr(III), Fe(III) and Ni(II) complexes had no activity against any species. By making comparison between the results of antifungal activity of the Schiff base ligand and its metal complexes, it was indicated that the ligand was biologically active against the fungus, *Candida albicans* with value 13.30 mm/mg. The Cd(II) complex was more potent fungicides than the parent ligand and standard antifungal drug (ketokonazole). The Cd(II) complex had fungicidal activity of 14.30 mm/mg against the same species. And this value of complex was more potent fungicides than the parent ligand and the standard drug (Ketokonazole). The other complexes showed no activity against *Candida albicans*.

The enhanced antimicrobial activity of all compounds against these organisms can be attributed to the concept of chelation. Because the positive charges of the metal were partially shared with the donor atoms found in the ligand and there was possible π-electron delocalization over the

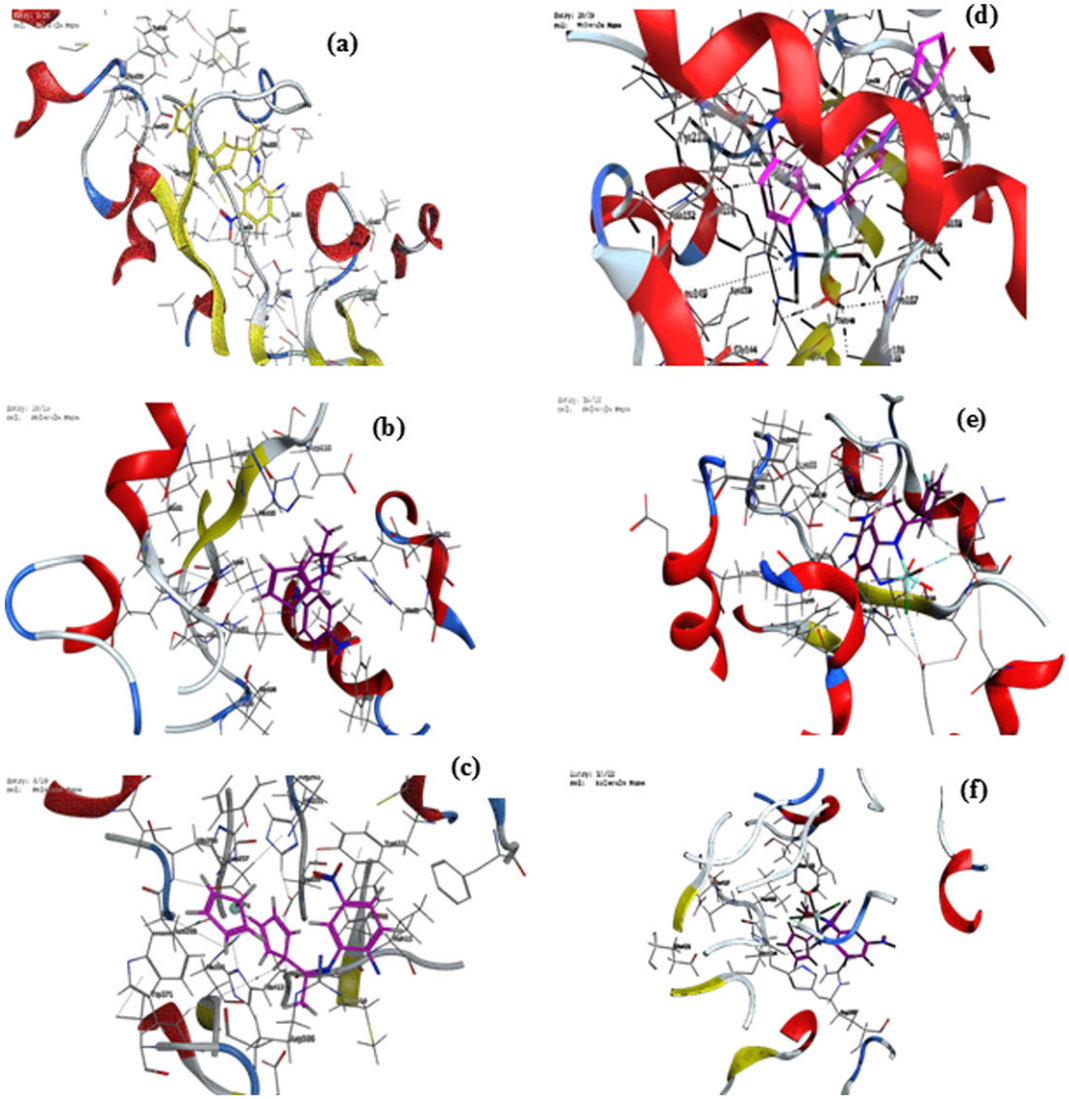

FIGURE 11 3D plot of the interaction between Schiff base ligand (L) with receptors of (a) 3HB5, (b) 3Q8U and (c) 5JPE and 3D plot of the interaction between $[Cd(L)(H_2O)_2Cl_2]$ complex with receptors of (d) 3HB5, (e) 3Q8U and (f) 5JPE

metal complex formed. The lipophilic character of the metal complex increases and supports its permeation more efficiently through the lipid layer of the micro-organisms. This permits easy binding and penetration of thecomplex in the cellular structure of the pathogens.[62] The chelation leads to make the ligand act as more powerful and potent bactereostatic agents. This inhibits the growth of bacteria more than the parent ligands. It was suspected that factors such as conductivity, solubility, dipole moment and cell permeability mechanism may be influenced by the presence of metal ion. This might be the possible reason for increasing the activity after chelation.[63,64]

5 | ANTICANCER ACTIVITIES

In various human diseases, cancer considered as the most severe disease to which humans were subjected and yet no effective drugs or any methods of control are available to treat it. So, it is necessary to identify novel, selective, potent and less toxic anticancer agents which became one of the most pressing problems. Cancer is a complex disease that is normally correlated to a wide range of escalating effects both at the cellular and molecular levels.[65] The cytotoxic ability of Schiff base ligand and its metal complexes were evaluated against breast carcinoma cells

TABLE 7 Energy values obtained in docking calculations of Schiff base ligand (L) and its Cd(II) complex with receptors of breast cancer mutant oxidoreductase (PDB ID: 3HB5), crystal structure of *Staphylococcus aureus* (PDB ID: 3Q8U) and yeast-specific serine/threonine protein phosphatase (PPZ1) of *Candida albicans* (PDB ID: 5JPE).

Compound	Receptor	Ligand moiety	Receptor site	Interaction	Distance (A°)	E (kcal mol^{-1})
Ligand (L)	3HB5	O 40	HZ LYS 159	H-acceptor	3.05	-1.30
		O 41	OH TYR 155	H-acceptor	3.07	-1.40
		O 41	NZ LYS 159	H-acceptor	2.97	-3.80
	3Q8U	O 41	NZ LYS 55	H-acceptor	3.48	-0.60
		Fe 10	OG1 THR 91	metal	2.14	-2.20
	5JPE	O 41	OH TYR 437	H-acceptor	2.98	-1.20
		C 15	5-ring HIS 413	H-π	3.79	-1.40
Cd (II) complex	3HB5	C29	OD1 ASN 152	H-donor	3.21	-1.60
		N36	OH TYR 155	H-donor	2.92	-15.30
		O44	OG SER 142	H-donor	2.98	-7.80
		O44	O CYS 185	H-donor	2.84	-1.80
		O44	O GLY 186	H-donor	3.12	-0.80
		O45	O GLY 186	H-donor	2.51	-7.10
		N26	OH TYR 155	Ionic	3.77	-1.00
		N36	OH TYR 155	Ionic	2.92	-5.00
		6-ring	6-ring	π-π	4.00	-0.00
	3Q8U	O 15	OD1 ASP 118	H-donor	3.14	-0.90
		C 30	ND1 HTS 115	H-donor	3.09	-1.30
		Cl 43	OE2 GLU 126	H-donor	3.03	-0.80
		O 45	OE2 GLU 51	H-donor	2.87	-15.20
		O 45	OD1 ASP 118	H-donor	2.63	-10.30
		Cl 50	O GLY 116	H-donor	2.89	-0.30
		O 40	OG1 THR 91	H-acceptor	3.04	-0.80
		O 40	NH1 ARG 102	H-acceptor	2.68	-2.20
		O 41	ND2 ASN 112	H-acceptor	2.71	-1.50
		N 26	OE1 GLU 51	Ionic	3.88	-0.80
		O 44	OD1 ASP 118	Ionic	3.13	-3.70
		O 44	OD2 ASP 118	Ionic	3.12	-3.70
		O 44	OE2 GLU 126	Ionic	3.92	-0.70
		O 45	OE1 GLU 51	Ionic	2.40	-10.00
		O 45	OE2 GLU 51	Ionic	2.87	-5.40
		O 45	OD1 ASP 118	Ionic	2.63	-7.50
		O 45	OD2 ASP 118	Ionic	3.88	-0.80
	5JPE	N 36	O HIS 413	H-donor	3.03	-5.30
		O 44	OD2 ASP 229	H-donor	2.88	-18.40
		O 44	OD2 ASP 257	H-donor	2.74	-5.70
		O 44	OD2 ASP 229	Ionic	2.88	-5.40
		O 44	OD2 ASP 257	Ionic	2.74	-6.50
		O 45	OD2 ASP 229	Ionic	3.17	-3.40

(MCF-7 cell line), which is one of the most common form of cancer. So firstly all the synthesized compounds screened against single dose experiment on MCF-7 cell line with concentration 100 μg/ml. The in vitro screening of the compounds showed that inhibition ratio for ligand is about 70 % and its metal complexes were found to be with inhibition ratio values between 45 and 74 %. The highest inhibition ratio value (74%) corresponding to Cd(II) complex. Also the relationship between drug concentration and cell viability was plotted to calculate IC_{50} (μg/ml) (the value which corresponds to the concentration required for 50% inhibition cell viability).[66] Furthermore, four concentrations (0, 12.5, 25 and 50 μg/ml) and the IC_{50} values of more active complexes with inhibition ratio value >70% were measured and listed in Table 6 and Figure 10. It was found that ligand (L) and its Co(II) and Cd(II) complexes had IC_{50} values = 50 μg/ml.[67] Also these active compounds were screened against single dose experiment on human normal melanocytes (HFB-4) cell line with concentration 100 μg/ml. It is shown that Cd(II) complex had the highest surviving ratio value of normal cells of about 59%. From these data, it is confirmed that $[Cd(L)(H_2O)_2Cl_2]$ complex can be considered as a very active drug and promising compound against breast cancer with lower side effect on normal cells than the others complexes. Due to its IC_{50}= 50 μg/ml, so the surviving human normal cells will be higher than 59%.

6 | MOLECULAR MODELING OF ORGANOMETALLIC SCHIFF BASE LIGAND (L) AND ITS CD(II) COMPLEX: DOCKING STUDY

Docking is a useful tool to suppose about the most preferred mode of binding of a small molecule to its target protein.[68] The focus of molecular docking is to simulate the molecular recognition process. One of the guides of molecular docking is to obtain an optimized conformation for each of the drug and protein with relative orientation between them such that the free energy of the overall system is minimized.[33] The calculated structure of the Schiff base ligand was docked with three possible biological targets: the receptors of breast cancer mutant oxidoreductase (PDB ID:3HB5), crystal structure of *Staphylococcus aureus* (PDB ID: 3Q8U) and yeast-specific serine/threonine protein phosphatase (PPZ1) of *Candida albicans* (PDB ID:5JPE). Three-dimensional plot curves of docking were shown in Figure 11. Also the binding energies of the ligand and Cd(II) complex with the three receptors were calculated using computational docking studies.[69] These energy values were listed in Table 7. The results showed that there are possible interactions between Schiff base ligand (L) and its Cd(II) complex

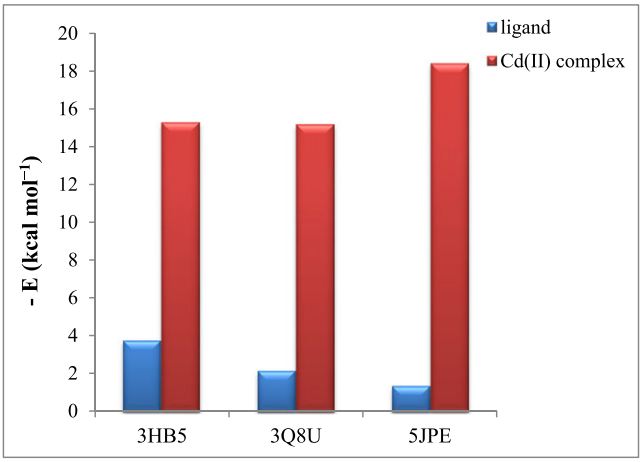

FIGURE 12 The relation between the lowest binding energy of the ligand and its Cd(II) complex with 3HB5, 3Q8U and 5JPE receptors

with 3HB5, 3Q8U and 5JPE receptors. The organometallic Schiff base ligand showed a stronger interaction with 3HB5 receptor than the other receptors with lowest binding energy -3.80 kcal mol^{-1}. The docking results detected that the main interaction force of the Schiff base ligand with the active sites were H-acceptor, H-Pi and metal. The lowest binding energies of the ligand and its Cd(II) complex with 3HB5, 3Q8U and 5JPE receptors were calculated and showed in Figure 12. The minimum binding energies were found to be −3.80, -2.20 and −1.40 kcal mol^{-1} for ligand and to be -15.30, -15.20 and -18.40 kcal mol^{-1} for $[Cd(L)(H_2O)_2Cl_2]$ complex with 3HB5, 3Q8U and 5JPE, respectively. From these data, it showed that Cd(II) complex was more interactive toward the receptors than the parent ligand. This may be due to the coordination with metal ions. Furthermore, it was concluded from the docking study for Cd(II) complex that there were favorable interaction with 3HB5,3Q8Uand 5JPE receptors. The strongest binding was with 5JPE receptor, it had the lowest binding energy value (-18.40 kcal mol^{-1}) than the other receptors.

7 | CONCLUSION

In the present study, the novel organometallic Schiff base ligand (L) and its Cr(III), Mn(II), Fe(III), Co(II), Ni(II), Cu(II), Zn(II)and Cd(II) complexes were prepared. The ligand synthesized by condensation reaction of 2-acetylferrocene with 4-nitro-1,2-phenylenediamine. These compounds were confirmed via various methods of analysis. The results obtained can be summarized as follows:

1. FT-IR spectra showed that the synthesized ligand behaved as a neutral bidentate ligand in all metal

complexes, in which it can form a coordinate bond with metal ions through azomethine nitrogen and NH_2 group.

2. Elemental analysis showed that reaction between ligand and metal ions occurred as 1:1 molar ratio and the complexes had the formulae of $[M(L)(H_2O)_2Cl_2].nCl.xH_2O$ if (M = Cr(III)) (n = 1) (x = 4); (M = Mn(II)) (n = 0) (x = 2); (M = Fe(III)) (n = 1) (x = 2); (M = Co(II)) (n = 0) (x = 3); (M = Zn(II)) (n= 0) (x = 1)) and (M = Cd(II)) (n = 0) (x = 0), and formulae of $[M(L)(H_2O)_3Cl].nCl.xH_2O$ if (M = Ni(II)) (n = 1) (x = 2); (M = Cu(II)) (n = 1) (x = 1). Also all complexes had octahedral structures.
3. The data indicated that Cr(III), Fe(III), Ni(II) and Cu(II) complexes were monomeric and 1:1 electrolytes while other complexes had non-electrolytic characters.
4. By screening some of the compounds against breast cancer cell line (MCF-7) and human normal melanocytes (HFB-4) cell line, it showed that Cd(II) complex can be considered as a very active drug against breast cancer with inhibition ratio (74%) with lower side effect on normal cells than the others.
5. The biological activity of the synthesized ligand and its complexes was studied against Gram (+) bacteria: [*Streptococcus mutans, Staphylococcus aureus],* Gram (−) bacteria: [*Escherichia coli, Klebsiella pneumonia, Pseudomonas aeruginosa*] and fungal specie include [*Candida albicans*]. It was found that the Zn(II), Cd(II) and Co(II) complexes had higher activities against all different bacterial species than the other complexes. Zn(II) complex had the highest activity value against *streptococcus mutans* specie. So, Zn(II) complex can be used as very active drug against this specie. But, each of Cr(III), Fe(III) and Ni(II) complexes had no activity against any species. Also, the Schiff base ligand and its Cd(II) complex were biologically active against the fungus, *Candida albicans*. While, other complexes were biologically inactive.
6. The geometrical structure for organometallic Schiff base ligand (L) was computed. From this, the binding energies, bond length and dipole moment were calculated. Also the data of experimental IR and UV-vis spectra were compared with theoretical ones, which showed that ligand was prepared successfully.
7. Molecular docking studies of the free organometallic Schiff base ligand (L) and its Cd(II) complex with receptors of (PDB ID: 3HB5, 3Q8U and 5JPE) detected that the ligand showed highest binding ability with binding energy of -3.80 kcal mol^{-1} with the receptor of breast cancer mutant oxidoreductase (PDB ID: 3HB5), while Cd(II) complex showed lowest binding energies -18.40 kcal mol^{-1} with the receptor 5JPE.

ORCID

Walaa H. Mahmoud http://orcid.org/0000-0001-9187-4325

REFERENCES

[1] M. M. Omar, H. F. Abd El-Halim, E. A. M. Khalil, *Appl. Organometal. Chem.* **2017**, In press.

[2] L. S. Pogany, J. Moncol, M. Gal, I. Salitros, R. Boca, *Inorg. Chim. Acta* **2017**, *462*, 23.

[3] M. Habibi, S. A. Beyramabadi, S. Allameh, M. Khashi, A. Morsali, M. Pordel, M. Khorsandi-Chenarboo, *Mol. Str.* **2017**, *1143*, 424.

[4] M. Anar, E. H. Ozkan, H. Ogutcu, G. Agar, I. Sakiyan, N. Sari, *Artificial Cells, Nanomedicine, and Biotechnology* **2016**, *44*, 853.

[5] E. Logoglu, E. A. Koyuncu, M. N. S. Karaboga, N. Sari, *Gazi Univer. J. Sci.* **2016**, *29*, 303.

[6] M. A. Diab, A. Z. El-Sonbati, A. F. Shoair, A. M. Eldesoky, N. M. El-Far, *Mol. Str.* **2017**, *1141*, 710.

[7] R. E. Kyne, M. C. Ryan, L. T. Kliman, J. P. Morken, *Org. Lett.* **2010**, *12*, 3796.

[8] J. Luan, L. Zhang, *Molecules* **2011**, *16*, 4191.

[9] T. J. Kealy, P. L. Pauson, *Nature* **1951**, *168*, 1039.

[10] Y. Liu, G. Lian, D. Yin, B. Su, *Spectrochim. Acta A* **2013**, *100*, 131.

[11] M. Shabbir, Z. Akhter, I. Ahmad, S. Ahmed, M. Bolte, H. Ismail, B. Mirza, *Inorg. Chim. Acta* **2017**, *463*, 102.

[12] B. Maity, M. Roy, B. Banik, R. Majumdar, R. R. Dighe, A. R. Chakravarty, *Organometallics* **2010**, *29*, 3632.

[13] R. W. Mason, K. McGrouther, P. R. R. Ranatunge-Bandarage, B. H. Robinson, J. Simpson, *Appl. Organometal. Chem.* **1999**, *13*, 163.

[14] C. Ornelas, *New J. Chem.* **2011**, *35*, 1973.

[15] A. A. Turki, *J. kerbala univ.* **2012**, *10*, 259.

[16] A. Albert, *Selective Toxicity: Physico-chemical Basis of Therapy (6th Edition)*, Wiley, New York **1979**.

[17] S. Chandra, D. Jain, A. K. Sharma, P. Sharma, *Molecules* **2009**, *14*, 174.

[18] P. Skehan, R. Storeng, D. Scudiero, A. Monks, J. McMahon, D. Vistica, J. T. Warren, H. Bokesch, S. Kenney, M. R. Boyd, *J. National Cancer Instit.* **1990**, *82*, 1107.

[19] M. J. Frisch, G. W. Trucks, H. B. Schlegel, G. E. Scuseria, M. A. Robb, J. R. Cheeseman, V. G. Zakrzewski, J. A. Montgomery, R. E. Stratmann, J. C. Burant, S. Dapprich, J. M. Millam, A. D. Daniels, K. N. Kudin, M. C. Strain, O. Farkas, J. Tomasi, V. Barone, M. Cossi, R. Cammi, B. Mennucci, C. Pomelli, C. Adamo, S. Clifford, J. Ochterski, G. A. Petersson, P. Y. Ayala, Q. Cui, K. Morokuma, D. K. Malick, A. D. Rabuck, K. Raghavachari, J. B. Foresman, J. Cioslowski, J. V. Ortiz, A. G. Baboul, B. B. Stefanov, G. Liu, A. Liashenko, P. Piskorz, I. Komaromi, R. Gomperts, R. L. Martin, D. J. Fox, T. Keith, M. A. Al-Laham, C. Y. Peng, A. Nanayakkara, C. Gonzalez, M. Challacombe, P. M. W. Gill, B. G. Johnson, W. Chen, M. W. Wong, J. L. Andres, M. Head-Gordon, E. S. Replogle, J. A. Pople, *GAUSSIAN 03 (Revision A.9)*, Gaussian, Inc., Pittsburgh **2003**.

[20] G. G. Mohamed, Z. H. Abd El-Wahab, *Spectrochim. Acta A.* **2005**, *61*, 1059.

[21] R. Dennington, T. Keith, J. Millam (Eds), *GaussView, Version 5.0.8, R*, KS: Dennington, Semichem Inc., Shawnee Mission **2009**.

[22] C. J. Dhanaraj, I. U. Hassan, J. Johnson, J. Joseph, R. S. Joseyphus, *J. Photochem. & Photobio. B* **2016**, *162*, 115.

[23] C. Balakrishnan, L. Subha, M. A. Neelakantan, S. S. Mariappan, *Spectrochim. Acta A* **2015**, *150*, 671.

[24] L. H. Abdel-Rahman, N. M. Ismail, M. Ismael, A. M. Abu-Dief, E. Abdel-Hameed, *Mol. Str.* **2017**, *1134*, 851.

[25] L. W. Jolly, *The Synthesis and Characterization of Inorganic Compounds*, Prentice-Hall, INC **1970** 485.

[26] N. M. Hosny, M. A. Husien, F. M. Radwan, N. Nawar, *Mol. Str.* **2017**, *1143*, 176.

[27] A. A. Maihub, A. M. Etorkil, S. M. Ben-Saber, M. M. El-ajaily, M. M. Abou-Krisha, *J. Chem. Eng.* **2014**, *8*, 226.

[28] W. H. Mahmoud, N. F. Mahmoud, G. G. Mohamed, A. Z. El-Sonbati, A. A. El-Bindary, *Mol. Str.* **2015**, *1095*, 15.

[29] S. R. Gupta, P. Mourya, M. M. Singh, V. P. Singh, *Organometal. Chem.* **2014**, *767*, 136.

[30] S. Adhikari, W. Kaminsky, M. R. Kollipara, *Organometal. Chem.* **2017**, *836*, 8.

[31] M. Dehkhodaei, M. Khorshidifard, H. A. Rudbari, M. Sahihi, G. Azimi, N. Habibi, S. Taheri, G. Bruno, R. Azadbakht, *Inorg. Chim. Acta* **2017**, *466*, 48.

[32] A. Z. El-Sonbati, M. A. Diab, S. M. Morgan, *J. Mol. Liq.* **2017**, *225*, 195.

[33] G. G. Mohamed, A. A. El-Sherif, M. A. Saad, S. E. A. El-Sawy, S. M. Morgan, *J. Mol. Liq.* **2016**, *223*, 1311.

[34] S. M. Morgan, A. Z. El-Sonbati, H. R. Eissa, *J. Mol. Liq.* **2017**, *240*, 752.

[35] A. Y. Al-Dawood, N. M. El-Metwaly, H. A. El-Ghamry, *J. Mol. Liq.* **2016**, *220*, 311.

[36] A. M. A. Alaghaz, M. E. Zayed, S. A. Alharbi, *Mol. Str.* **2015**, *1083*, 430.

[37] N. Okulik, A. H. Jubert, *Internet Electron. J. Mol. Des.* **2005**, *4*, 17.

[38] H. Wang, X. Zhang, Y. Zhao, D. Zhang, F. Jin, Y. Fan, *Mol. Str.* **2017**, *1148*, 496.

[39] B. Annaraj, S. Pan, M. A. Neclakantan, P. K. Chattaraj, *Comput. Theor. Chem.* **2014**, *1028*, 19.

[40] Z. Parsaee, K. Mohammadi, *Mol. Str.* **2017**, *1137*, 512.

[41] S. Roy, K. Harms, S. Chattopadhyay, *Polyhedron* **2016**, In Press.

[42] W. H. Mahmoud, N. F. Mahmoud, G. G. Mohamed, *J. Therm. Anal. Calorim.* **2017**, In Press.

[43] H. Vural, M. Orbay, *Mol. Str.* **2017**, *1146*, 669.

[44] N. Mishra, K. Poonia, S. K. Soni, D. Kumar, *Polyhedron* **2016**, *120*, 60.

[45] W. H. Mahmoud, N. F. Mahmoud, G. G. Mohamed, *J. Coord. Chem.* **2017**, In press.

[46] Z. Beigi, A. H. Kianfar, G. Mohammadnezhad, H. Görls, W. Plass, *Polyhedron* **2017**, *134*, 65.

[47] N. Ribeiro, S. Roy, N. Butenko, I. Cavaco, T. Pinheiro, I. Alho, F. Marques, F. Avecilla, J. C. Pessoa, I. Correia, *J. Inorg. Biochem.* **2017**, *174*, 63.

[48] E. M. Zayed, G. G. Mohamed, A. M. M. Hindy, *J. Therm. Anal. Calorim.* **2015**, *120*, 893.

[49] A. A. Abdel Aziz, I. S. A. El-Sayed, M. M. H. Khalil, *Appl. Organometal. Chem.* **2017**, In Press.

[50] Y. Shi, H. Yang, W. Shen, C. Yan, X. Hu, *Polyhedron* **2004**, *23*, 15.

[51] S. Yadav, R. V. Singh, *Spectrochim. Acta A* **2011**, *78*, 298.

[52] G. Y. Nagesh, B. H. M. Mruthyunjayaswamy, *J. Mol. Str.* **2015**, *1085*, 198.

[53] H. F. Abd El- Halim, G. G. M. , M. N. Anwar, *Appl Organometal Chem.* **2017**, In press.

[54] S. Velumania, X. Mathew, P. J. Sebastian, S. K. Narayandass, D. Mangalaraj, *Sol. Energ. Mat. Sol. C.* **2003**, *76*, 347.

[55] S. Basavaraja, D. S. Balaji, M. D. Bedre, D. Raghunandan, P. M. P. Swamy, A. Venkatarman, *Bull. Mat. Sci.* **2011**, *34*, 1313.

[56] N. K. Poonia, S. Siddiqui, M. D. Arshad, D. Kumar, *Spectrochim. Acta A* **2016**, *155*, 146.

[57] M. I. Khan, A. Khan, I. Hussain, M. A. Khan, S. Gul, M. Iqbal, I. R. F. Khuda, *Inorg. Chem. Comm.* **2013**, *35*, 104.

[58] A. M. A. Alaghaz, M. E. Zayed, S. A. Alharbi, *Mol. Str.* **2015**, *1084*, 36.

[59] T. D. Thangadurai, K. Natarajan, *Indian J. Chem. A* **2001**, *40*, 573.

[60] Z. H. Chohan, H. Pervez, A. Rauf, K. M. Khan, C. T. Supuran, *J. Enzyme Inhib. Med. Chem.* **2004**, *19*, 417.

[61] S. Gopalakrishnan, R. Rajameena, E. Vadivel, *Drug Res.* **2012**, *4*, 31.

[62] G. More, D. Raut, K. Aruna, S. Bootwala, *J. Saudi Chem. Soc* **2017**, In Press.

[63] Z. H. Chohan, M. Praveen, *Appl. Organometal. Chem.* **2001**, *15*, 617.

[64] Z. H. Chohan, C. T. Supran, A. Scozzafava, *J. Enz. Inhib. Med. Chem.* **2004**, *19*, 79.

[65] S. J. Kirubavathy, R. Velmurugan, R. Karvembu, N. S. P. Bhuvanesh, I. V. M. V. Enoch, P. M. Selvakumar, D. Premnath, S. Chitra, *Mol. Str.* **2017**, *1127*, 345.

[66] C. M. Sharaby, M. F. Amine, A. A. Hamed, *Mol. Str.* **2017**, *1134*, 208.

[67] M. A. Arafath, F. Adam, M. R. Razali, L. E. A. Hassan, M. B. K. Ahamed, A. M. S. A. Majid, *Mol. Str.* **2017**, *1130*, 791.

[68] S. Mondal, S. M. Mandal, T. K. Mondal, C. Sinha, *Mol. Str.* **2017**, *1127*, 557.

[69] J. Tang, J. Liu, *Bioorg. Chem.* **2016**, *69*, 29.

How to cite this article: Mahmoud WH, Deghadi RG, Mohamed GG. Metal complexes of novel Schiff base derived from iron sandwiched organometallic and 4-nitro-1,2-phenylenediamine: Synthesis, characterization, DFT studies, antimicrobial activities and molecular docking. *Appl Organometal Chem*. 2018;e4289. https://doi.org/10.1002/aoc.4289